Characterization and Performance of the Electroosmotic Pumping Effect for Different Porous Media

By

Daniel Piwowar

A thesis submitted to the

Graduate School-New Brunswick

Rutgers, The State University of New Jersey

In partial fulfillment of the requirements

For the degree of

Master of Science

Graduate Program in Mechanical and Aerospace Engineering

Written under the direction of

Professor F. Javier Diez

and approved by

_____

_____

_____

_____

New Brunswick, New Jersey

October, 2012

ABSTRACT OF THE THESIS

Characterization and Performance of the Electroosmotic Pumping Effect for Different Porous Media

by Daniel Piwowar

Thesis Director:

Professor F. Javier Diez

High flow rate electroosmotic, EO, pumps are of great interest due to their simple design and non-moving parts. EO pumps were fabricated from two types of membranes: a never before tested, microcapillary array and the popular, anodic aluminum oxide (AAO). Flow rates and power consumption were measured directly for both membranes while efficiency was measured indirectly for the AAOs. A normalized flow rate of 1.90 mL/min/V/cm^2 was recorded which is the highest normalized flow rate published. Large inefficiencies can occur due to electrolysis and electrode spacing and thus methods to decreasing these problems are discussed. Electroosmotic pumps were driven by constant voltage and asymmetric voltage pulses. The asymmetric voltage pulses negated electrolysis while producing a net flow. Voltage losses due to electrode spacing were minimized by platinum coatings.

Acknowledgements

I would first like to thank Dr. F. Javier Diez for giving me the opportunity to work in the electrokinetics field and providing a challenging research area. He provided insight and direction when I needed it the most and showed the utmost patience when I challenged the boundaries of graduate school. Thank you again for always finding time to talk to me about the details of my research and life itself.

I wish to also extend my thanks to my thesis committee members, Dr. Shahab Shojaei Zadeh, a professor of Mechanical Engineering at Rutgers University and Dr. Jerry Shan, professor of Mechanical Engineering at Rutgers University, for their valuable time spent evaluating this thesis and assisting in its completion.

I want to thank John Petrowski and Joseph Vanderveer of the Mechanical Engineering Department at Rutgers University for helping with any electrical or manufacturing questions I had. Their combined experience filled in my lack of knowledge in said fields and thoroughly increased my productivity. Also I want to extend my thanks to Dr. Zadeh for the excellent fluids classes and expert advice and to Dr. Hao Lin for the in-depth Fluids III class.

I want to thank the endless knowledge of Andrew Miller. He was the first to guide me through electrokinetics and provided expert knowledge and experience on the subject. We have had our differences at times but it was a pleasure working with him. I am indebted to countless hours I spent talking to Josh Shawala. His vast knowledge of electrokinetic theory helped conceive the many experiments I have done for this thesis.

His outlook on life and the advice he has given me helped me more than he knows. Thank you for being my friend. I also want to thank Tom Hansen for working with me during the first stages of my prototype. He provided excellent machining skills and a resourcefulness that is hard to find. I wish him best of luck in his future endeavors.

Finally, I want to thank my friends for all their support and the many distractions that go with graduate school: Sean DeGennaro, Mike Fechtmann, Matt Ambrusch, Tom Reesbeck, Mariusz Zarzecki, Cevat Akin, and Arturo Villegas from Rutgers University. Also, thank you to my friends outside of Rutgers that helped me keep sane and on track: Bob Booth, Dan Carson, Tor Holste, Jay Adragna, Andrew Fabian, Phil Unto, Paul Abbazia, Pete Austin, and last but not least Diana Pearl.

Daniel Piwowar

Rutgers University

August 6, 2012

Table of Contents

List of Figures

List of Tables

List of Symbols

Symbol	Description	Units
a	Pore Radius	m
A_{el}	Electrode Area	m^2
A_{mem}	Membrane Area	m^2
b	Voltage Factor	
C	Integration Constant	
c_i	Ion Concentration	M
D	Electrode Distance	m
e	Electron Charge	C
E_z	Electric Field	Vm^{-1}
F	Ion Drag Force per Volume	Nm^{-3}
G	Hydraulic Resistance	$Pasm^{-3}$
I	Current	A
j_{cond}	Conduction Current Density	Am^{-2}
j_{conv}	Convection Current Density	Am^{-2}
k	Boltzmann Constant	$m^2kgs^{-2}K^{-1}$
l	Length	m
M	Electroosmotic Characteristic	$Am^{-1}Pa^{-1}$
N	Membrane Pore Number	
N_A	Avogadro's Number	mol^{-1}
P	Pressure	Nm^{-2}
P_z	Pressure Gradient	Nm^{-3}
Q	Flow Rate	m^3s^{-1}
R	Electrical Resistance	Ω
r	Radial Position	m
R_{el}	Electrode Spacing Resistance	Ω
R_{mem}	Membrane Resistance	Ω
R_{total}	Total Pump Resistance	Ω
t	Time	s
T	Temperature	K
u	Velocity	ms^{-1}
V	Voltage	V
V_{an}	Anode Voltage	V

V_{app}	Applied Voltage	V
V_{cat}	Cathode Voltage	V
V_{dec}	Decomposition Voltage	V
V_{eff}	Effective Voltage	V
V_o	Overpotential	V
Vol	Volume per pulse	m^{-3}
z	Valence Number	
ε	Permittivity of Liquid	Fm^{-1}
ζ	Zeta Potential	V
η	Viscosity	Nsm^{-2}
Θ	Porosity	
κ	Inverse Debye Length	m^{-1}
Λ	Conductivity	Sm^{-1}
λ_D	Debye Length	m
ξ	Voltage of Pulse	V
ρ	Charge Density	Cm^{-3}
ψ	Potential	V
χ	Efficiency	%
$\tilde{r} = \kappa r$	Dimensionless Radial Position	
$\Psi = \frac{e\psi}{kT}$	Dimensionless Potential	
Ψ_H	Dimensionless High Potential	
Ψ_L	Dimensionless Low Potential	
$\tilde{\zeta} = \frac{e\zeta}{kT}$	Dimensionless Zeta Potential	
$\tilde{r}^*$	Radial Position when $\Psi_L = \Psi_H = 1$	

Subscript	
-	negative pulse
+	positive pulse
an	anode
app	applied
aq	aqueous
cat	cathode
cond	conduction
conv	convection
D	Debye
eff	effective
el	electrode
g	gas
H	High
L	Low
max	maximum
mem	membrane
z	thickness gradient

Chapter 1.

Introduction

1.1. Review of Electrokinetics

Electrokinetics involves the study of fluid motion due to the interaction of an electric field. It encompasses the four fields of electroosmosis, electrophoreisis, streaming potential, and sedimentation potential [1]. Of the four fields, the study of electroosmosis is the basis of this thesis. When a surface, such as a capillary tube, is charged or becomes charged from its interaction with an aqueous solution, an electric double layer exists and forms the basis for electroosmotic flow. When there is an applied electric field, ion migration towards an electrode in this double layer will cause viscous drag and create a net flow throughout the charged porous material.

The electric double layer forms from the migration of ions to a charge surface. Counterions are first attracted to form a thin stationary layer called the stern layer next to the charged surface [2]. Due to charge imbalance, a second layer of ions forms to balance the excess charge due to Coulomb's Law. This second layer comprised mostly of coions forms a larger dispersed layer called the diffuse layer. The two layers combine to form what is known as the Debye length shown empirically by

$$\lambda_D = \frac{1}{\kappa} = \left(\frac{\varepsilon kT}{N_A e^2 \sum_{i=\infty}^{N} z_i^2 c_i} \right)^{1/2} \qquad (1.1.1)$$

Due to the charged surface, a potential is thus formed inside the channel. At the shear surface, approximately at the boundary of the stern and diffuse layer, the zeta potential is defined. The zeta potential is an important characteristic for electroosmotic flow within a material. As shown the Chapter 2, the zeta potential will become an important factor in defining flow rate, pressure generation, and efficiency.

1.2. Electroosmotic Pump and Its Applications

Electroosmotic pumps refer to the movement of a fluid to create a desirable flow rate or pressure change due to electroosmosis. Theses pumps can be created using a variety of methods from capillaries packed with silica [3][4][5] to porous membranes[6][7][8][9]. Electroosmotic pumps have several advantages compared to typical mechanical pumps. The advantages include no moving parts, no mechanical parts, and a simple design. Electroosmotic pumps have been used in a variety of applications including power electronic cooling [10], fuel cells [11], actuation [12], drug delivery [13], chromatography [14], and lab on chip systems [15]. The theoretical basis for electroosmotic pumping is presented below.

1.3. Motivation

As discussed previously, electroosmotic pumps have been used in a variety of applications that require a variety of pumping conditions. High flow rates are one condition that is of high interest. To obtain high flow rates, the use of large electric fields are needed but two continuing problems have been voltage losses due to pump resistance

and faradaic reactions resulting in gas generation which can decrease efficiency and cause pore blockage. The objective of this study was to create high flow rate electroosmotic pumps with the reduction of pump resistance and to develop a method to eliminate gas generation at the electrodes.

1.4. Thesis Outline

Chapter 2 defines the theory of electroosmosis. It starts by defining the velocity profile obtained by electroosmosis and then describes the potential across a cylindrical pore. By combining the velocity and potential profiles, pumping characteristics can be defined such as flow rate, pressure, power consumption, and efficiency. Chapter 3 discusses the loss of voltage and efficiency due to faradaic reactions and pump resistance. It also discusses methods of eliminating these losses and defines a new method of asymmetric voltage pulsing to drive the fluid. Chapter 4 sums up the experimental details including pump housing, membrane descriptions, and aqueous solutions used. Chapter 5 discusses in detail the pumping characteristics of the membranes and the effects of asymmetric voltage pulsing. Chapter 6 presents the main conclusions from this work.

Chapter 2.

Electroosmotic Pump Theory

The basis for electro-osmotic flow in cylindrical pores for high zeta potentials was outlined in Levine et al [16]. Levine et al was able to lift the restriction of low zeta-potential values from [17]. In the following sections, electroosmotic pump theory is defined. Flow characteristics are first modeled in cylindrical coordinates and then the potential due to an electrical double layer is modeled and compared. Maximum flow rates and maximum pressure is then defined with current consumption following. Finally the efficiency is defined and methods of obtaining a membrane's zeta potential.

2.1. Velocity Profile

The charge density can be modeled by the Poisson's equation assuming a 1:1 electrolyte as

$$\rho(r) = -\frac{\varepsilon}{r}\frac{d}{dr}\left(r\frac{d\psi}{dr}\right) \qquad (2.1.1)$$

The boundary conditions are as follows

$$\psi(a) = \zeta \qquad (2.1.2)$$

$$\left.\frac{d\psi(r)}{dr}\right|_{r=0} = 0 \qquad (2.1.3)$$

The Navier-Stokes equation can be first reduced by assuming steady, low Reynolds number flow with the added presence of both an axial pressure field and axial electric field to find the velocity. It is written as

$$\frac{1}{r}\frac{d}{dr}\left(r\frac{du}{dr}\right)=-\frac{P_z}{\eta}-\frac{\rho(r)}{\eta}E_z \qquad (2.1.4)$$

By using the boundary conditions of

$$u(a)=0 \qquad (2.1.5)$$

$$\left.\frac{du(r)}{dr}\right|_{r=0}=0 \qquad (2.1.6)$$

the equation can be integrated twice to produce the velocity profile which is

$$u(r)=\frac{1}{4\eta}\left(a^2-r^2\right)P_z-\frac{\varepsilon}{\eta}\left(\zeta-\psi(r)\right)E_z \qquad (2.1.7)$$

For zero pressure gradients and small potentials, the velocity equation reduces to the Helmholtz-Smoluchowski equation as follows

$$u=-\frac{\varepsilon\zeta}{\eta}E_z \qquad (2.1.8)$$

2.2. Potential Profile

The induced potential in a pore can be described using the Poisson-Boltzmann equation

$$\frac{1}{\tilde{r}}\frac{d}{d\tilde{r}}\left(\tilde{r}\frac{d\Psi\left(\tilde{r}\right)}{d\tilde{r}}\right)=\sinh\Psi\left(\tilde{r}\right) \qquad (2.2.1)$$

with boundary conditions of

$$\Psi(\kappa a) = \tilde{\zeta} \tag{2.2.2}$$

$$\left.\frac{d\Psi(\tilde{r})}{d\tilde{r}}\right|_{\tilde{r}=0} = 0 \tag{2.2.3}$$

Rice & Whitehead [17] were able to solve the Poisson-Boltzmann equation to calculate the potential by using the Debye-Huckel equation which limits the potential to low values, specifically 25.4mV or lower. Levine et al [16] developed a solution for the potential for any potential values such as 100mV or more. Their idea was to break the potential down into two zones: a high and low potential region. They used the findings from [18] to approximate the hyperbolic sine function by two separate functions:

$$\sinh\Psi = \Psi \qquad 0 \le \Psi \le 1 \tag{2.2.4}$$

$$\sinh\Psi = \frac{1}{2}\exp(\Psi) \qquad \Psi > 1 \tag{2.2.5}$$

It can be graphically represented by Fig. 1. They were then able to separate the potential equations into the following

$$\frac{1}{\tilde{r}}\frac{d}{d\tilde{r}}\left(\tilde{r}\frac{d\Psi_L(\tilde{r})}{d\tilde{r}}\right) = \Psi_L(\tilde{r}) \qquad 0 \le \tilde{r} \le \tilde{r}^* \tag{2.2.6}$$

$$\frac{1}{\tilde{r}}\frac{d}{d\tilde{r}}\left(\tilde{r}\frac{d\Psi_H(\tilde{r})}{d\tilde{r}}\right) = \frac{1}{2}\exp\left(\Psi_H(\tilde{r})\right) \qquad \tilde{r}^* \le \tilde{r} \le \kappa a \tag{2.2.7}$$

with boundary conditions of

$$\Psi_L(\tilde{r}^*) = \Psi_H(\tilde{r}^*) = 1 \tag{2.2.8}$$

$$\left.\frac{d\Psi_L(\tilde{r})}{d\tilde{r}}\right|_{\tilde{r}=\tilde{r}^*} = \left.\frac{d\Psi_H(\tilde{r})}{d\tilde{r}}\right|_{\tilde{r}=\tilde{r}^*} \qquad (2.2.9)$$

The solutions for the potential can be separated in four subdomains. Subdomain I was characterized by the Debye-Huckel approximation. The next three subdomains are characterized by the integration constant obtained by integrating Eq. (2.2.5). This integration constant helps identify the importance of the inner low-potential and outer high-potential regions.

$$C = \left[2 + \tilde{r}^* \frac{I_1(\tilde{r}^*)}{I_0(\tilde{r}^*)}\right]^2 - e\tilde{r}^{*2} \qquad (2.2.10)$$

Our experimental results produced potentials characterized by subdomains I, IIA, and III. The potential solutions of the subdomains are in Table 1.

Subdomain	C	Inner Low Potential $\Psi_L(\tilde{r}) =$	Outer High Potential $\Psi_H(\tilde{r}) =$
I	N/A	$\tilde{\zeta}\frac{I_0(\tilde{r})}{I_0(\kappa a)}$	0
IIA	< 0	$\frac{I_0(\tilde{r})}{I_0(\tilde{r}^*)}$	$\ln\left[\frac{-C}{\tilde{r}^2\cos^2\left(B_- + \frac{1}{2}\sqrt{-C}\ln\left(\frac{\tilde{r}}{\kappa a}\right)\right)}\right]$
IIB	4 > C > 0	$\frac{I_0(\tilde{r})}{I_0(\tilde{r}^*)}$	$\ln\left[\frac{4B_+C\left(\frac{\tilde{r}}{\kappa a}\right)^{\sqrt{C}}}{\tilde{r}^2\left(1-B_+\left(\frac{\tilde{r}}{\kappa a}\right)^{\sqrt{C}}\right)^2}\right]$
III	C = 4	0	$\ln\left[\frac{16B_+}{(\kappa a)^2\left(1-B_+\left(\frac{\tilde{r}}{\kappa a}\right)^2\right)^2}\right]$

Table 1. Channel potential equations.

With the following parameters $B_- = \cos^{-1}\sqrt{\frac{-C}{e^{\tilde{\zeta}}(\kappa a)^2}}$ and $B_+ = \frac{\sqrt{C+e^{\tilde{\zeta}}(\kappa a)^2}-\sqrt{C}}{\sqrt{C+e^{\tilde{\zeta}}(\kappa a)^2}+\sqrt{C}}$.

2.3. Flow Rate and Pressure

To find the volumetric flow rate of the system, the velocity can be integrated over the cross sectional area of the channel to give

$$Q = 2\pi \int_0^a ru(r)dr = \frac{\pi a^4}{8\eta} P_z - \frac{\varepsilon \zeta \pi a^2 f}{\eta} E_z \qquad (2.3.1)$$

where [19]

$$f = \int_0^a \left(1 - \frac{\psi(r)}{\zeta}\right) \frac{2r}{a^2} dr \qquad (2.3.2)$$

f was defined by Levine et al [16] to "compare the mean electrostatic potential to the ζ". *f* tends to unity for large κa values. From the flow rate equation, the maximum flow rate occurs when the back pressure is zero. Maximum pressure occurs when the flow rate equals zero. Setting the appropriate values reveal

$$Q_{\max} = -\frac{\varepsilon \zeta \pi a^2 f}{\eta} E_z \qquad (2.3.3)$$

$$P_{z,\max} = -\frac{8\varepsilon \zeta f}{a^2} E_z \qquad (2.3.4)$$

Q_{max} and P_{max} are linearly related to the applied electric field and zeta potential and thus increasing either one will increase the maximum flow rate or maximum pressure.

2.4. Current

The current density is made up of two components: conduction and convection. The conduction current is due to the movement of ions relative to the bulk fluid and is derived

from Ohm's Law. Using a Boltzmann ion distribution and assuming an equimobile electrolyte [16], the conduction current is

$$j_{cond} = \Lambda \cosh\left(\frac{ze\psi}{kT}\right) E_z \qquad (2.4.1)$$

The conduction current density can be further reduced if the surface conductance is sufficiently small. This occurs when κa is much larger than 1 or for low potential values as suggested by [17]. Thus the current density can be represented by the solution's conductivity as seen in

$$j_{cond} = \Lambda E_z \qquad (2.4.2)$$

The convection current is the transport of ions through the bulk fluid by its velocity and can be written as

$$j_{conv} = \rho(r)u(r) \qquad (2.4.3)$$

The total current is calculated by integrating the total current density over the entire channel giving

$$I = 2\pi \int_0^a r\left(j_{cond} + j_{conv}\right) dr \qquad (2.4.4)$$

This can also be written as [19]

$$\begin{aligned} I = \frac{\pi a^2 \varepsilon \zeta P_z}{\eta} \int_0^a \left(1 - \frac{\psi}{\zeta}\right) \frac{2r}{a^2} dr + \frac{\pi a^2 \varepsilon^2 E_z}{\eta} \int_0^a \left(\frac{d\psi}{dr}\right)^2 \frac{2r}{a^2} dr \\ + \pi a^2 \Lambda E_z \int_0^a \frac{2r}{a^2} \cosh\left(\frac{ze\psi}{kT}\right) dr \end{aligned} \qquad (2.4.5)$$

Yao et al [19] would go on to create a dimensionless ratio of the flow rate to the current consumption by creating

$$g = f \Bigg/ \left\{ \frac{\varepsilon^2}{\eta \Lambda} \int_0^a \left(\frac{d\psi}{dr} \right)^2 \frac{2r}{a^2} dr + \int_0^a \cosh\left(\frac{ze\psi}{kT} \right) \frac{2r}{a^2} dr \right\} \qquad (2.4.6)$$

Where g would tend to unity at large κa values.

2.5. Onsager Relation

In 1951, Mazur and Overbeek laid the foundation to the linear regime for electroosmotic flow using the Onsager reciprocal theorem [20]. According to Ohm's Law, the current of a system is linearly proportional to the applied voltage. According to Darcy's Law, a flow rate is linearly proportional to a pressure gradient in a microfluid system. It is also true according to the electroosmotic effect that fluid flow can be caused by an applied voltage and a pressure gradient can cause a potential known as the streaming potential which in turn creates its own current. These effects can be related by using the Onsager relation and combining Eq. (2.3.1) and Eq. (2.4.4). To simplify the presentation, a matrix is typically used [21][22] as such

$$\begin{bmatrix} Q \\ I \end{bmatrix} = - \begin{bmatrix} 1/G & M \\ M & 1/R \end{bmatrix} \begin{bmatrix} P \\ V \end{bmatrix} \qquad (2.5.1)$$

G is termed the hydraulic resistance which describes the ability of the liquid to flow through the channel. R is termed the electrical resistance of the liquid in the channel. M describes the electroosmotic behavior from which flow is induced by voltage and current is induced by flow. M has been verified within 10% for electroosmotic pumps by [23].

2.6. Efficiency

The efficiency of electroosmotic pumps is defined in the usual manner of mechanical pumps by the hydraulic output power compared to the electrical input power and is thus

$$\chi = \frac{QP}{IV} \qquad (2.6.1)$$

In the sense of Eq. (2.6.1), the flow rate with the normal back pressure would be combined with the applied voltage (not the effective voltage) and the measured current to produce an efficiency value. Typical measurements for electroosmotic pumps are usually maximum flow rate and maximum pressure and thus Chen et al [24] showed the efficiency is thus a quarter of the combination of the maximum flow rate and maximum pressure or

$$\chi = \frac{Q_{\max} P_{\max}}{4IV} \qquad (2.6.2)$$

2.7. Zeta Potential

To help determine theoretical values for electroosmotic pumping and to quantify membrane characteristics, the zeta potential of the membrane needs to be calculated. First and foremost, single channel theory needs to be updated to include multiple channels. This is easily done by comparing the open area of the membrane to the single pore area which will calculate the number of pores in the membrane as

$$N = \frac{\Theta A_{mem}}{\pi a^2} \qquad (2.7.1)$$

Flow rate and current calculations for single channel theory can now be multiplied by N to achieve the respected values.

The zeta potential can now be calculated by using a variety of methods. Cao et al [9] summarized the three methods of obtaining the zeta potential of membranes. The first two methods were described by Reichmuth et al [25] which used the measured maximum pressure or maximum flow rate as

$$\frac{P_{\max}}{V_{eff}} = -\frac{8\varepsilon\zeta}{a^2} \qquad (2.7.2)$$

$$\frac{Q_{\max}}{V_{eff}} = -\frac{N\pi a^2 \varepsilon\zeta}{\eta l} \qquad (2.7.3)$$

Both of these equations assume a negligible f value and constant zeta potential, permittivity, and viscosity values. The zeta potential then can be found from the respective graphs by calculating the slope. Yao et al [6] were able to extract the zeta potential by measuring the maximum flow rate and maximum current concurrently and graphing their results as

$$\frac{Q_{\max}}{I_{\max}} = -\frac{\varepsilon\zeta}{\eta\Lambda} g \qquad (2.7.4)$$

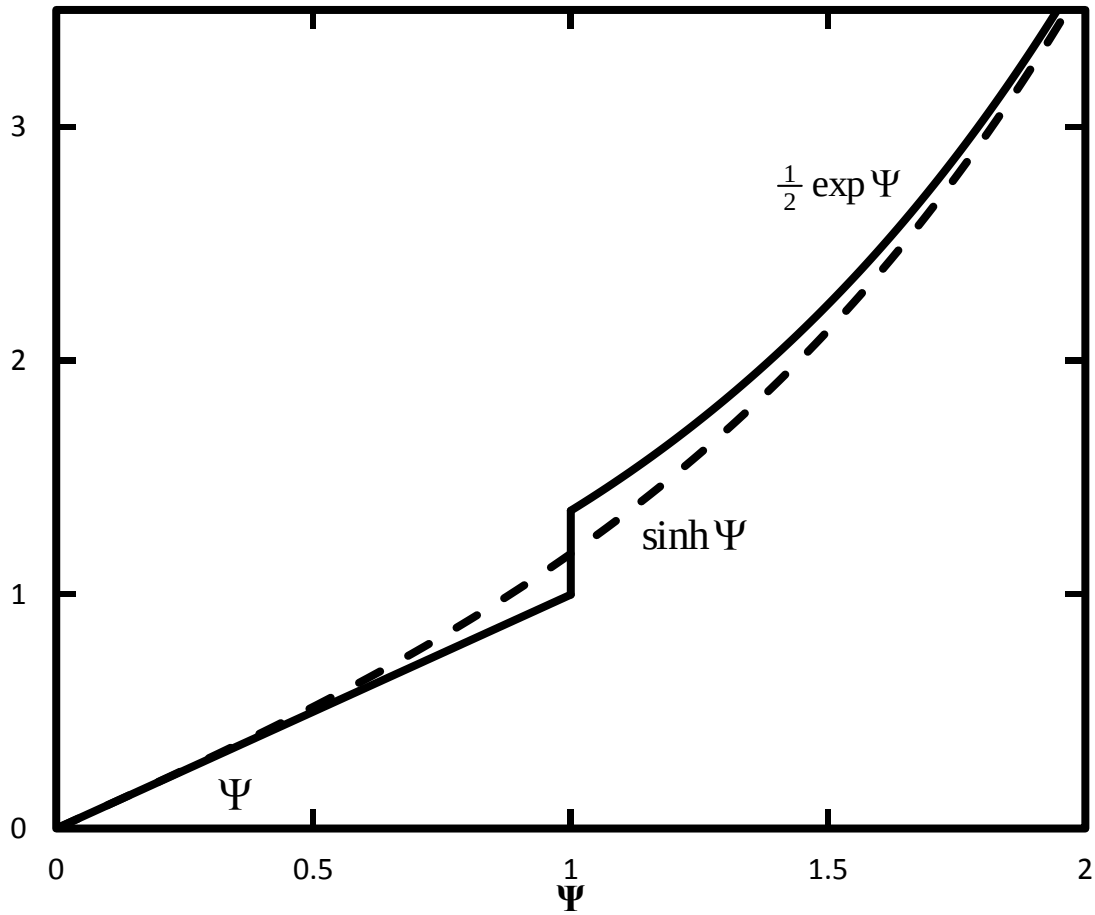

Fig. 1. Graphical representation of Eq. (2.2.4) and Eq. (2.2.5) from [16].

Chapter 3.

Efficiency Loss

The two main reasons for efficiency loss for electroosmotic pumps are faradaic reactions and voltage losses. As in an electrolytic cell, when two electrodes are placed in an aqueous solution with a sufficient amount of power, faradaic reactions occur and can result in gas evolution, pH changes, and electrode degradation. Voltage losses due to electrode spacing can be substantial. Even a spacing of a few millimeters can result in 75% loss in voltage across the membrane. The faradaic reactions are first explained and a literature survey is done on the methods to decrease these reactions. A new way of cancelling faradaic reactions is next described by using asymmetric voltage pulses. Finally, voltage losses are explained and methods of calculating the effective voltage across a membrane are defined.

3.1. Faradaic Reactions

Gas evolution, also known as electrolysis, occurs at the electrodes and can decrease the efficiency and increase the possibility of channel blockage. To combat a pH change, large reservoirs can be used but are not practical for on chip devices. To negate electrode erosion, many electroosmotic pumps utilize platinum electrodes due to their high inert properties. Nevertheless, they still produce bubbles from the reaction of hydrogen and oxygen at the cathode and anode, respectively, and given by

$$2H^{+}_{(aq)} + 2e^{-} \rightarrow H_{2(g)} \qquad (3.1.1)$$

$$2H_2O \rightarrow O_{2(g)} + 4H^+_{(aq)} + 4e^- \qquad (3.1.2)$$

One method of reducing this reaction is to stay below the voltage limit of the reaction [26], approximately 2V. This method is impractical for high flow rate electroosmotic pumps. Several other methods have been proposed. Many electroosmotic pumps have employed ion exchange membranes, meshes, or other devices to simply block the bubbles from entering the pores [10][27][6]. This has been proven effective but leaves the device with an overload of gases or the need for platinum catalysts for recombination. Lin et al [28] used Nafion tubing to funnel the gases out of the electroosmotic pump into a recombineder to create H_2O. Some electroosmotic pumps have deviated away from the inert electrodes and went with disintegrating electrodes as in Heuck et al [29]. Their explanation was to accept the erosion due to their short term usage but to negate the large bubble production. Others have turned to using palladium electrodes [30] due to their hydrogen absorbing properties although this is only effective for small quantities of hydrogen gas typically produced in de-ionized water. Another idea was to include additives to the solution to reduce the hydrogen and oxygen reaction at the electrodes as did Kohleyer et al [31]. For large volume electroosmotic pumps, this may be impractical.

A shift in thinking has developed for the idea of pulsing the voltage or current. Electrolysis is dependent on the amount of current supplied at the electrodes. If the current was reversed fast enough to stop the hydrogen/oxygen reaction, no gas would form. Selvaganapathy et al [32] used a zero net current pulse to stop the electrolysis but with different time lapses of the positive and negative side. This uneven time difference allowed a net positive flow and showed evidence of no gas evolution. Xu et al [23] used positive voltage pulsing to digitally control the flow. They found that bubble formation

was delayed to approximately 5 minutes and it was found to be an effective way to stabilize the flow rate. Finally others have proposed using AC [33] to decrease the electrolysis. This has been proven successful but requires the electrodes to be placed along the channel (i.e., inside the pores) thus not allowing for small pore size and small length. In the next section, asymmetric voltage pulsing will be presented to negate bubble production but produce a net flow.

3.2. Asymmetric Voltage Pulses Theory

It has been shown that using asymmetric voltage pulses as seen in Fig. 2, a net fluid flow can be established and faradaic reactions can be stopped due to equal area pulsing. By confining the area per pulse to be equal, the net current is zero and thus faradaic reactions are cancelled. Stuetzer et al [34] proved the basis for this motion. He first related the force on a space charge as

$$F = \rho E \qquad (3.2.1)$$

The pressure developed across a pore can be inferred from the Navier Stokes equation by

$$P = \int_{r_1}^{r_2} \rho E ds \qquad (3.2.2)$$

Stuetzer further simplifies the equation by using Maxwell's equation

$$\frac{dE}{dx} = \frac{\rho}{\varepsilon} \qquad (3.2.3)$$

Therefore the pressure becomes the following with the electrodes orthogonal to the pump axis at x = 0 and x = l

$$P = \frac{\varepsilon}{2} E^2 \Big|_0^l \qquad (3.2.4)$$

Steutzer briefly showed that the maximum pressure can be approximated by the maximum electric field occurring at the collecting electrode which is

$$P_{\max} = \frac{\varepsilon}{2} E_{\max}^2 \qquad (3.2.5)$$

Combining Eq. (2.3.1) from electroosmotic theory and Eq. (3.2.5) reveals

$$Q = -\frac{\pi a^4}{8\eta} \frac{\varepsilon V^2}{2l^3} - \frac{\varepsilon \zeta a^2 (1-G)}{\eta} \frac{V}{l} \qquad (3.2.6)$$

The flow rate is thus divided into two separate parts that contribute to fluid motion. The right hand side from the classical electroosmotic theory keeps its linear relationship while the left hand side follows a quadratic relationship. McBride [35] used the quadratic relationship between pressure and electric field to produce a net fluid flow by asymmetric voltage pulses as seen in Fig. 3. He started by relating the positive and negative pressure fields to the respective pulses

$$P_+ \approx \frac{\xi_+^2}{l^2} \qquad (3.2.7)$$

$$P_- \approx \frac{\xi_-^2}{l^2} \qquad (3.2.8)$$

He then related the flow rate caused by the pressures and assuming a constant fluid resistance, the volume of liquid for the positive and negative pulses are comparable by

$$\frac{\xi_+^2}{\xi_-^2} = \frac{Q_+}{Q_-} = \frac{Vol_+ / t_+}{Vol_- / t_-} \qquad (3.2.9)$$

He further set up the voltage pulses to have equal areas under the following conditions

$$\xi_+ t_+ = \xi_- t_- \qquad (3.2.10)$$

$$\xi_+ = b\xi_- \qquad (3.2.11)$$

$$t_+ = \frac{1}{b} t_- \qquad (3.2.12)$$

By combining Eq. (3.2.9) and the previous conditions, the ratio of volume produced by each pulse can be compared thus

$$Vol_+ = bVol_- \qquad (3.2.13)$$

Therefore applying equal area but asymmetric voltage pulses will provide a net flow rate proportional to the voltage factor. Referring back to Fig. 3, the classical electroosmotic flow rate creates a much larger volume than the quadratic voltage relation when the voltages are below 10kV but keeps bubble production to a minimum.

3.3. Voltage Loss

Another source of efficiency loss is the voltage drop between an electrode and the membrane due to the surrounding fluid. Following Yao et al [6] description of effective pump voltage, the effective voltage across the membrane is not the applied voltage. There are two major sources of voltage reduction: electrode decomposition voltage and the voltage drop through the solution from the electrodes to the membrane. The decomposition voltage combines the voltage needed for the reactions at the cathode and the anode and the overpotential voltage needed to start the process.

$$V_{dec} = V_{cat} - V_{an} + V_o \qquad (3.3.1)$$

This decomposition voltage is dependent on the molarity of the reactants, the chemical composition of the electrodes and reactants, and the amount of current supplied. It can be measured indirectly by taking the slope intercept of I-V curves. V_{dec} tends to be small where [6] found a value of 4V for 1mM borate buffer. The voltage drop occurring between the electrodes and the membrane can be calculated by

$$R_{el} = \frac{D}{A_{el}\Lambda} \qquad (3.3.2)$$

It can also be found experimentally by removing the membrane and taking the slope of an I-V curve. Yao et al [6] combined these results and the experimental current to calculate the effective voltage as

$$V_{mem} = V_{app} - V_{dec} - 2IR_{el} \qquad (3.3.3)$$

Another method of calculating the effective voltage is to obtain the total resistance of the pump from the I-V curve and to calculate the membrane resistance as

$$R_{mem} = \frac{l_{mem}}{\Theta A_{mem}\Lambda} \qquad (3.3.4)$$

The membrane resistance can be obtained experimentally by subtracting the electrode spacing resistance from the total resistance. These two values can be combined as follows [9]

$$V_{mem} = \frac{R_{mem}}{R_{total}}\left(V_{app} - V_{dec}\right) \qquad (3.3.5)$$

To increase the effective voltage, electrodes need to be placed as close as possible to the membrane. Miao et al [36] was able to sputter platinum onto the faces of their AAOs which effectively eliminates the voltage loss due to electrode spacing.

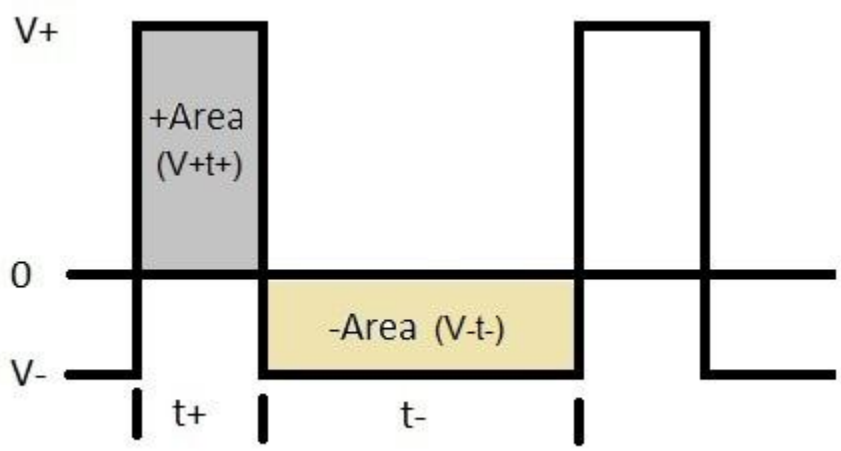

Fig. 2. A sketch of the applied asymmetric voltage pulses that drive an electroosmotic pump. The positive and negative areas are equal to cancel faradaic reactions.

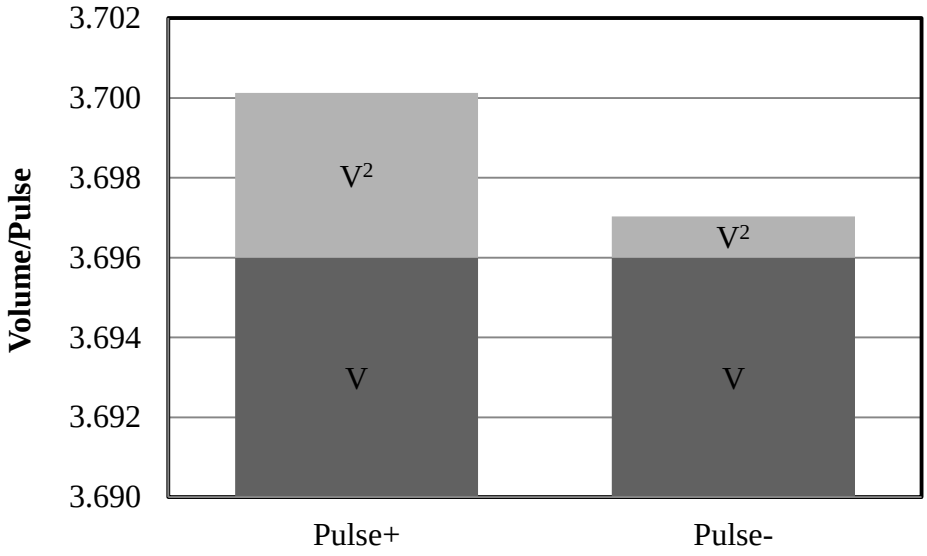

Fig. 3. The volume attained from a single voltage pulse. As shown in Eq. (3.2.6), a greater amount of fluid is moved by the linear relationship but has a net cancelation over the entire cycle. The quadratic relationship has a net flow but at a significant reduction in volume.

Chapter 4.

Electroosmotic Pump Characteristics

The electroosmotic pump is first described along with methods of obtaining pump performance. Following are the descriptions of the two membranes studied. Finally, the aqueous solutions used in the experiments are explained in detail.

4.1. Pump Housing and Measurements

The electroosmotic pump housing was created from acrylic blocks machined to make four milliliter internal reservoirs as seen in Fig. 4. Plastic barbed tube fittings were used to connect the inner reservoirs to large diameter outer reservoirs using ¼" PVC tubing for flow rate measurements. A scale (Ohaus Scout Pro ±0.001g) monitored the output flow as seen in Fig. 5. Due to high pressures, the tubing was eliminated and brass fittings were used to connect the pressure transducer (Omegadyne PX309) for maximum pressure measurements as seen in Fig. 6. Silicone rubber gaskets were used to seal the pump. Membranes were epoxied to PVC sheets of 0.8mm thickness to hold the membranes inside the housing. Platinum wire and mesh were used as electrodes for the electroosmotic pump. Using inert platinum electrodes allow the lifetime of the pump to not be dependent on the electrode degradation. Platinum wire (99.9% pure) of 0.25mm diameter and platinum 52 mesh (99.9% pure) were obtained from Sigma Aldrich. A Keithley 6517B electrometer or a Trek model 5/80 amplifier with a Tektronix AFG 3021B function generator was used to supply power to the electroosmotic pump.

4.2. Membranes

4.2.1. Microcapillary Arrays

Glass microcapillary arrays were obtained from INCOM. These arrays were made of borosilicate glass with a chemical composition of 72% SiO_2, 12% B_2O_3, 7% Al_2O_3, 6% Na_2O, 2% K_2O, and 1% CaO. They had a pore diameter of 10 μm with a porosity of 60%, tortuosity of 1, and thickness of 1mm as seen in Fig. 7. These arrays have never been evaluated, to the best of the author's knowledge, for use in electroosmotic pumps. The microcapillary arrays had a typical exposed area of 3.65 cm^2.

4.2.2. Anodic Aluminum Oxide

Anodic aluminum oxide (AAO) membranes were obtained from Synkera Technologies, Inc with a pore size of 150nm and a 50 μm membrane thickness as seen in Fig. 8. These membrane characteristics include symmetric cylindrical pore radius throughout the thickness of the membrane, porosity of 30% - 32%, and tortuosity of 1.These membranes can be used with working fluids with pH in the range of 5 – 8 but if they are heat treated up to 1000^oC they can be operated in the range of 4.7 – 9. Chen et al [7] have shown the zero zeta potential to be at pH 8 with a positive zeta potential less than 8 and a negative zeta potential above 8. A zeta potential of +80mV was reported in Chen et al [37] for a pH ~6.5 while at pH ~9 a zeta potential of -15 to -35mV was reported. To increase the low zeta potentials at higher pH levels, Vajander et al [38] coated their AAOs with a 5nm layer of SiO_2. This coating was predicted to increase the zeta potential to ~-104mV at pH

~9. A custom coating of 10nm of SiO_2 was thus added to the heat treated AAOs by atomic layer deposition. Miao et al [36] coated their AAOs with a layer of Pt on both faces to act as electrodes whereby maximizing the effective voltage. A 100nm Pt coating was thus added to SiO_2 coated AAOs to achieve this same effect. An average exposed area for the AAOs were 0.400 cm^2.

4.3. Aqueous Solutions

The primary solutions used were deionized water and phosphate buffer. Deionized ultra-filtered water was obtained from Fischer Scientific (W2-20). Phosphate buffer was made using the deionized ultra-filtered water and the combination of Sodium Phosphate Monobasic (≥99% pure) and Sodium Phosphate Dibasic (≥99% pure) each obtained from Sigma Aldrich. Phosphate buffer was made into varying molarities with a constant pH of 6.2. The corresponding phosphate buffer conductivities are listed in Table 2 with the deionized water conductivity measured to be 1.51μS/cm. Conductivity and pH measurements were conducted using an Oakton 510 series meter. A borate buffer solution was also used in conjunction with the microcapillary arrays. The borate buffer was made using deionized ultra-filtered water and the combination of Boric Acid (99% pure) and Sodium Tetraborate (99% pure) each obtained from Sigma Aldrich. Molarites of 1 and 2 mM were produced with a constant pH of 8.7.

mM	pH	Conductivity (μS/cm)
0.1	5.68	6.23
0.5	6.10	45
1	6.21	90
2	6.29	168
10	6.30	861

Table 2. Phosphate buffer conductivity

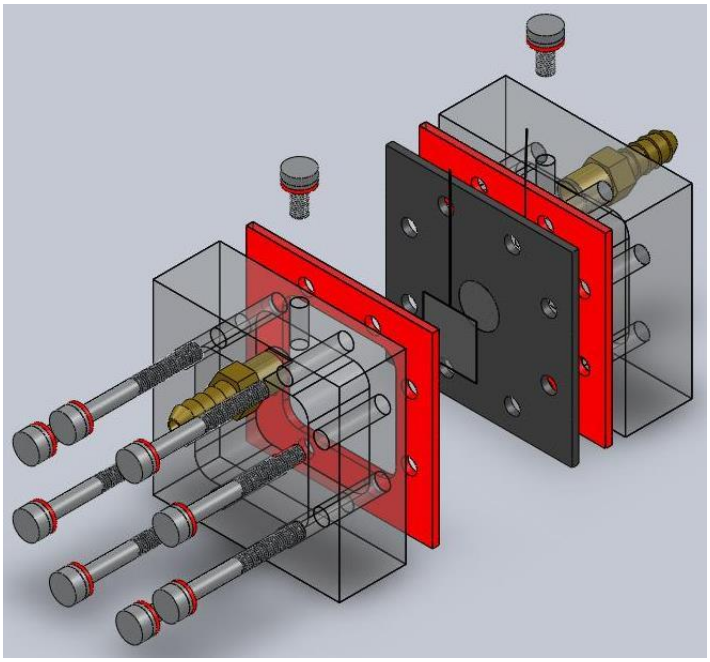

Fig. 4. A 3D model of the electroosmotic pump housing.

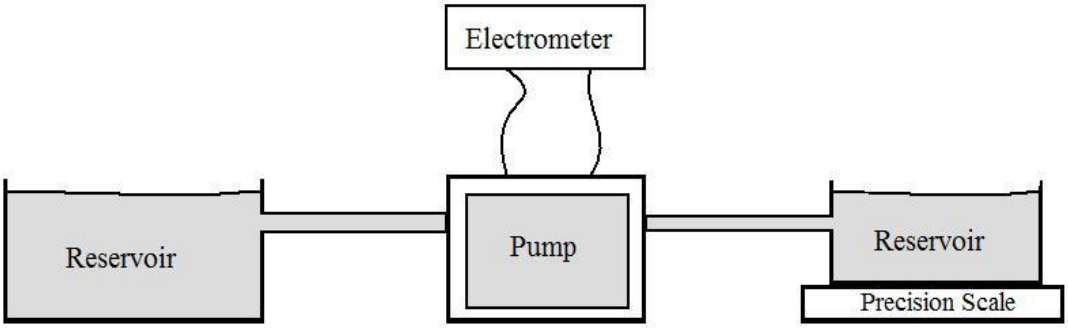

Fig. 5. A sketch showing the experimental setup for flow rate measurements.

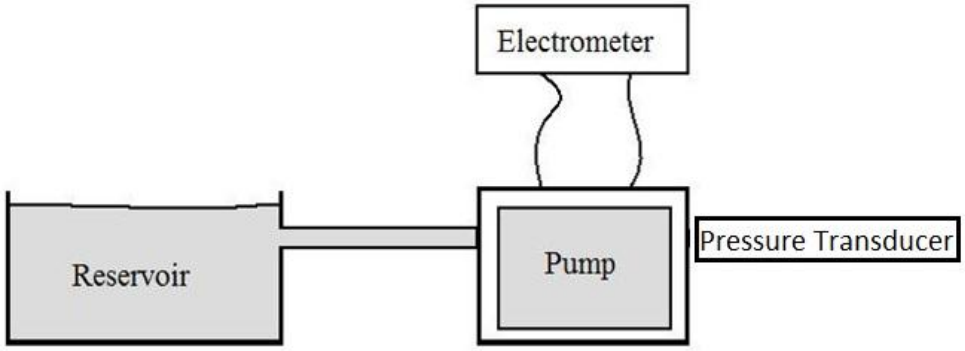

Fig. 6. A sketch showing the experimental setup for pressure measurements.

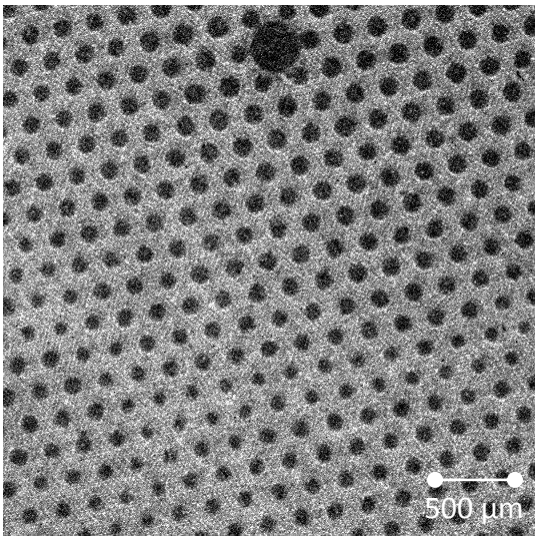

Fig. 7. A photo of the microcapillary arrays.

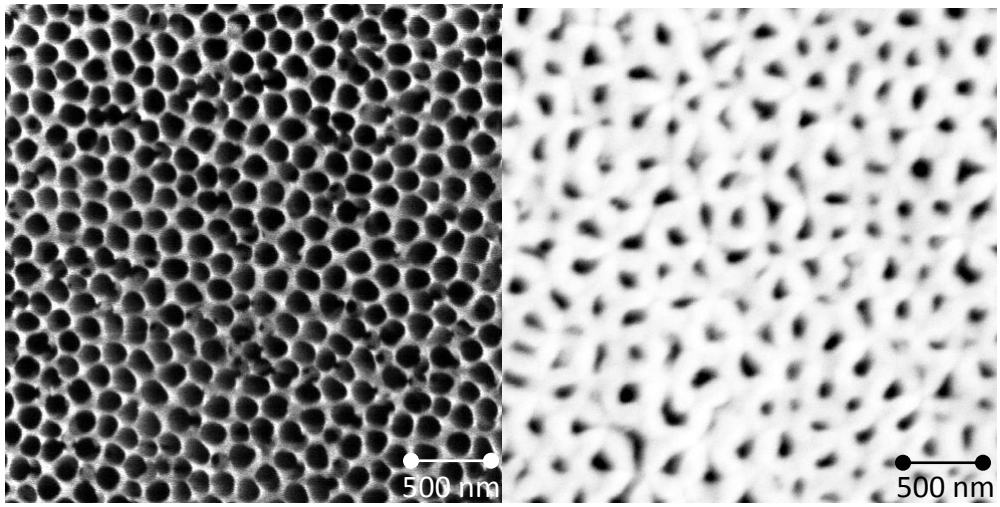

Fig. 8. SEM images of an untreated AAO (Left) and an AAO with SiO_2 and platinum coatings (Right).

Chapter 5.

Electroosmotic Pump Performance

The present work evaluates the capabilities of membranes to generate electroosmotic flow. This will be shown by characterizing their electroosmotic pumping performance. An important parameter that can affect the pump performance is the characteristics of the applied voltage. The analysis will first show the effect of a constant applied voltage on the maximum flow rate, current consumption, maximum pressure, zeta potentials of the membranes, and efficiency. To enhance the capabilities of the pump, the applied voltage is asymmetrically pulsed to which the maximum flow rate, power consumption, maximum pressure, efficiency, and temperature increase are also evaluated.

5.1. Constant Voltage

5.1.1. Flow Rate / Power Consumption

The ability of electroosmotic pumps to achieve high flow rates is highly desirable and is useful for a variety of applications; therefore high flow rate generation is evaluated. Using the setup as described in Fig. 5, flow rate measurements were conducted for the microcapillary arrays, SiO_2 coated AAOs, and SiO_2 coated and Pt coated AAOs. To compare the flow rates of the membranes to each other and published results, this is normalized by the applied voltage and open area of the membrane. This normalized flow rate now includes the membrane characteristics (voltage, area, and thickness) and can be

plotted against the applied electric field as shown in Fig. 9. The advantage of plotting the results in terms of the applied electric field and not the effective electric (which removes voltage losses), is that includes both the actual pump's power consumption and its effective electric field.

The first membranes to be evaluated were the 10μm pore microcapillary arrays. These microcapillary arrays achieved a maximum flow rate of 5.38mL/min but due to its large area it produces a normalized flow rate of 0.049 mL/min/V/cm^2. The microcapillary arrays can benefit from reduction of their thickness and pore size. Reducing a membrane's thickness effectively increases its electric field which in turn increases its flow rate. The microcapillary arrays' κa value of 614 for 1 mM buffers shows a large pore size compared to the small Debye length. As summarized in [24], a κa greater than 100 becomes ineffective in producing a larger flow rate and thus reducing the pore size would decrease any loss due to inefficient viscous drag. The flow rated generated by the microcapillary arrays increases when using borate buffer instead of phosphate buffer as shown in Fig. 10. Considering that both solutions have the same molarity, this performance improvement is due to the increase of zeta potential. This increases is due to the change in pH from 6.2 for phosphate buffer to 8.7 for borate buffer. The various calculated zeta potentials are shown in Table 4. Along with an increase in flow rate, the current consumption is much lower for the borate buffer than the phosphate buffer as shown in Fig. 11 due to the increased conductivity of the phosphate buffer.

The second type of membranes to be evaluated were the SiO_2 coated AAOs. In terms of normalized flow rate, they are comparable to the SiO_2 coated AAOs from [38] and the porous silicon membranes from [8]. The SiO_2 coated AAOs achieved a maximum flow

rate of 0.561 mL/min at 30V which corresponds to a 0.102 mL/min/V/cm^2 normalized flow rate. The measured flow rates of the SiO_2 coated AAOs are similar to the theoretical predictions as shown in Fig. 12. Similarly, the measured current consumption is linear with the applied voltage and with the molarity of the solutions as predicted by the theory and shown in Fig. 13. The effect of the molarity on the flowrate is shown in Fig. 14. This figure compares the flow rates generated by varying the molarity of the phosphate buffer using the SiO_2 coated AAOs. Fig. 14 shows that molarities greater than 2mM do not contribute to a significant increase in flow rate. This is comparable to the result obtained by [38] where a 2.5mM solution generated their greatest normalized flow rate. As discussed by [38], in the regime of $10 \geq \kappa a \geq 1$, flow rate decreases as the electric double overlaps. Present results have the same tendency with 1mM phosphate buffer ($\kappa a = 8$) having a greater flow rate than a 0.1mM phosphate buffer ($\kappa a = 2$).

The best performing electroosmotic pump utilized a SiO_2 coated AAO with a Pt coating on both of its faces. The platinum coating negates any voltage loss from the electrodes to the membrane and thus allows the applied voltage to be approximately equal to the effective voltage. The SiO_2 and Pt coated AAOs' flow rate improved by an order of magnitude compared with the non Pt coated AAOs and outperformed the SiO_2 and Pt coated AAOs from [36]. The SiO_2 and Pt coated AAOs obtained a flow rate of 2.10 mL/min at 10V which equates to a 1.90 mL/min/V/cm^2 normalized flow rate. To our knowledge this normalized flow rate is the highest obtained o date.

5.1.2. Pressure

Another method for comparing the performance of electroosmotic pumps is their

efficiency. As discussed in section 2.6, this requires measuring the electroosmotic pumps' maximum pressure. The measurements were conducted using the setup described in Fig. Fig. 6 to obtain the efficiency for the SiO_2 coated AAOs. A 1mM phosphate buffer was used due to the higher flow rates obtained previously. Results are compared to published data in Fig. 15. This figure shows that the SiO_2 coated AAOs allow a greater maximum pressure than the APS coated AAOs from [37]. It should be noted that the pore size difference of 150nm to 200nm may be affecting the total performance. As noted by [24] and shown by Eq. (2.3.4), smaller pore sizes tend to produce a greater maximum pressure.

5.1.3. Zeta Potential and Dimensionless *f* and *g*

Quantifying the zeta potential is an important step in determining the characteristics of an electroosmotic pump. As discussed earlier, a higher zeta potential will result in a higher flow rate. Furthermore, knowing a membrane's zeta potential is needed for predicting its maximum performance. Theoretically, the zeta potentials for the microcapillary arrays and the SiO_2 coated AAOs should be approximately the same as borosilicate glass capillaries due to similar chemical composition. Therefore the method from [39] was first used to determine the typical zeta potential for borosilicate glass capillaries with 1mM borate buffer, 1mM phosphate buffer, and 0.1mM phosphate buffer. The results are shown in Table 3. Zeta potentials for the microcapillary arrays and the SiO_2 coated AAOs were determined using Eq. (2.7.4).

The microcapillary arrays are constructed out of borosilicate glass and should be similar to the glass capillaries. The microcapillary arrays' zeta potential of -60mV for borate

buffer and -14mV for phosphate buffer was lower than expected as compared to -104mV and -97mV from the literature listed in Table 3. Table 4 shows the calculated zeta potential of the microcapillary arrays for the four buffer studied. The low zeta potentials may be due to differences in chemical composition between the microcapillary arrays and the single channels [40]. The chemical composition of the borosilicate glass channels is 81% SiO_2, 13% B_2O_3, 4% Na_2O+K_2O, and 2% Al_2O_3. A 9% difference in SiO_2 may be a contributing factor for the zeta potential change. Zeta potential calculations using Eq. (2.7.4) have been proven effective in [6] but with large error and thus needs to be considered.

The 10nm SiO_2 coating on the AAOs is expected to give the same zeta potential as the borosilicate glass. The SiO_2 coated AAOs had a lower than expected zeta potential as seen in Table 5. The SiO_2 coating created a negative zeta potential for the phosphate buffer for which non-coated AAOs' zeta potential would have been positive as explained earlier. Looking back at Table 3, 1mM phosphate buffer would exhibit a zeta potential of -97mV, whereas a zeta potential of -13.4mV was observed. It is therefore concluded that the SiO_2 coating was not as affective and must be altered to increase the performance capabilities of the AAOs.

As described in the previous sections, the dimensionless numbers f and g described the correction factor needed for electroosmotic flow and a ratio of flow to current consumption, respectively. As seen in Table 6, the microcapillary arrays demonstrate that at large κa values, f and g tends towards unity. The SiO_2 coated AAOs with a 1mM buffer shows that these dimensionless correction factors need to be taken into account when describing the flow. The f and g values have been plotted in Fig. 16. For comparisons to

[19], ζ_s = -3.8 and β = 8.8.

5.1.4. Efficiency

Comparing electroosmotic pumps by their efficiency, relates the total fluid output to the total electrical input power. By using Eq. (2.6.2), the efficiency of the coated AAOs can be calculated. Table 7 contains the calculated efficiencies and recent published results. Comparing the SiO_2 coated AAOs to varying coatings of [37], the latter had much higher efficiencies that can be attributed to their lower current consumption. A higher current consumption could be caused by the differences in conductivity and pump resistance. The same decrease in efficiency can be seen with the SiO_2 and Pt coated AAOs and [36] although conductivity and pump resistance were similar. Further investigation will be needed to resolve the difference.

5.2. Asymmetric Voltage Pulses

5.2.1. Flow Rate / Power Consumption

As previously discussed, asymmetric voltage pulsing has the advantage of decreasing or effectively eliminating faradaic reactions at the electrodes but experimentally proving a net flow rate for electroosmotic pumps utilizing membranes has never been published. As with constant voltage electroosmotic pumps, the maximum flow rate is a desired performance characteristic. Using the same setup as before, flow rate measurements were obtained. Fig. 17 shows the measured flow rates using the SiO_2 coated AAOs with three

different area comparisons. By changing the positive and negative pulse areas, the flow rate is driven by the greater area voltage. As previously found using constant voltage, 1mM phosphate buffer allows a greater flow rate than 0.1mM phosphate buffer. As shown in the theory, the use of equal area pulses create a net flow but its significantly less than a flow produced from constant voltage. By creating an imbalance in the area of the pulses, the linear voltage theory no longer cancels each volume out per pulse but creates a much higher net flow. This imbalance does produce a small amount of faradaic reactions but not to the extent of constant voltage. It was also found that changing the frequency from 100 to 500 to 1000Hz made no difference to the flow rate as expected. Higher frequencies were not tested due to amplifier limitations. The highest flow rates observed for 0.1mM and 1mM phosphate buffer are seen in the inset of Fig. 17 were 2.95mL/min at +1800/-900V and 1.69mL/min at +400/-200V, respectively.

As with all electroosmotic pumps, power consumption is an important characteristic. By changing the voltage factor, described as the volume ratio between the positive and negative pulse, varying degrees of input power are experimented with. Fig. 18 shows that a 2:1 voltage factor has the best flow rate to power consumption. Comparisons can then be made of power consumption to flow rate for the asymmetric voltage pulsing and constant voltage as seen in Fig. 19. It shows that the asymmetric voltage pulsing follows the same type curves as the constant voltage but is not as efficient. The least efficient method or the worst performer in terms of power to flow rate is the equal area pulsing which has been shown early in Fig. 17.

5.2.2. Pressure

As with constant voltage analysis, pressure measurements are needed to calculate the efficiency. Pressure measurements were done using 1mM phosphate buffer for SiO_2 coated AAOs to calculate the efficiency. Fig. 21 shows, as expected, the increase in pressure due to the increase in power consumption. It also shows that the pressure was maximized for equal areas at about 2.1 kPa for +200/-50V. As in the case of flow rates, pressure was again maximized with a greater negative area to positive area.

5.2.3. Efficiency

Efficiency measurements are needed to quantify not only the differing pulse areas but also to compare to constant voltage. The calculated efficiencies are plotted in Fig. 22. As expected, the equal area pulses are very inefficient but by changing the area ratios, the efficiency increases by two magnitudes. The greater negative area pulsing is the most efficient and is only one order of magnitude lower than a constant voltage pump. Increasing to a greater negative ratio will undoubtedly increase the efficiency but will cause more faradaic reactions. It is therefore concluded that a balance of efficiency and acceptable electrode reactions must be considered.

5.2.4. Temperature

Temperature fluctuations in electroosmotic pumps can be a significant factor in output performance. Temperature is known to change several fluid characteristics including viscosity, permittivity, and conductivity. Potential in a channel can also be affected as

described in Eq. (2.2.1). Monitoring fluid temperature is simply done by extracting fluid from the pump and measuring the temperature with a thermocouple. No significant increase in temperature was recorded for constant voltage flow rates from 10 to 30V. For asymmetric voltage pulses, there was a temperature increase at high voltages as seen in Fig. 23. As the input power increased, temperature increased as well. This increase in temperature is most likely due to Joule heating between the electrodes. A simple experiment was conducted in which the membrane was removed and temperature was recorded. This resulted in approximately the same temperature rise.

Solution	Zeta (mV)	Zeta (mV) Reference
1mM BB	-104	-104 [8]
1mM PB	-97	~-90 [41]
0.1mM PB	-120	~-100 [41]

Table 3. Borosilicate glass zeta potentials

Membrane	Solution	Zeta Potential (mV)
Microcapillary array	1mM PB	-14.1
Microcapillary array	2mM PB	-10.9
Microcapillary array	1mM BB	-60.3
Microcapillary array	2mM BB	-59.6

Table 4. Microcapillary zeta potential

Membrane	Phosphate Molarity	Zeta Potential (mV)
AAO SiO_2	0.1	-0.5
AAO SiO_2	0.5	-7.8
AAO SiO_2	1	-13.4
AAO SiO_2	2	-13.2
AAO SiO_2	10	-21.4

Table 5. AAO SiO_2 zeta potential

Membrane	Solution	κa	f	g
Microcapillary array	1mM Phosphate Buffer	614	.997	.963
AAO SiO2	1mM Phosphate Buffer	8	.766	.212

Table 6. *f* and *g* values for membranes

Source	Coating	Efficiency (%)
Present	SiO_2	0.028
Present	SiO_2,Pt	0.161
[36]	SiO_2,Pt	0.900
[37]	APS	0.100
[24]	None	0.430

Table 7. Efficiency for coated AAOs

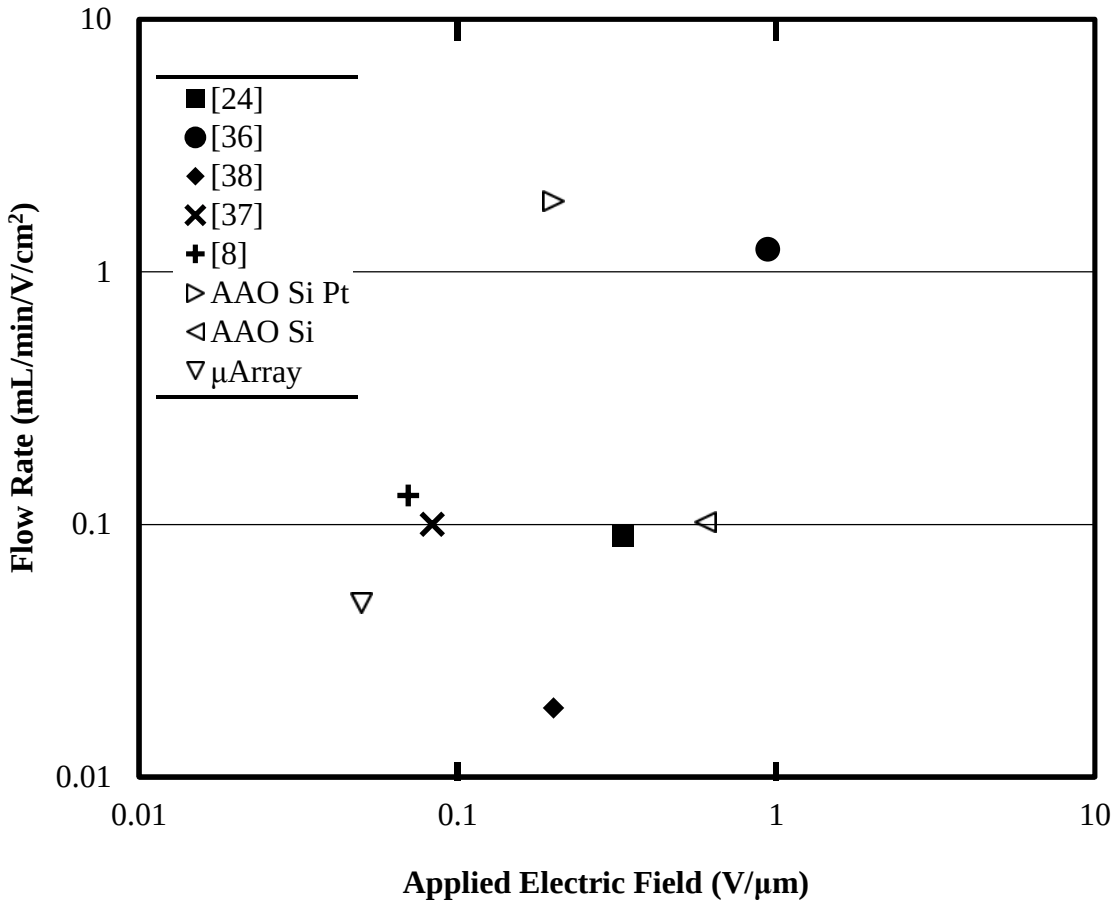

Fig. 9. Normalized flow rate plotted against the applied electric field. Platinum coated AAOs allowed for maximum effective electric field and thus the highest normalized flow rate.

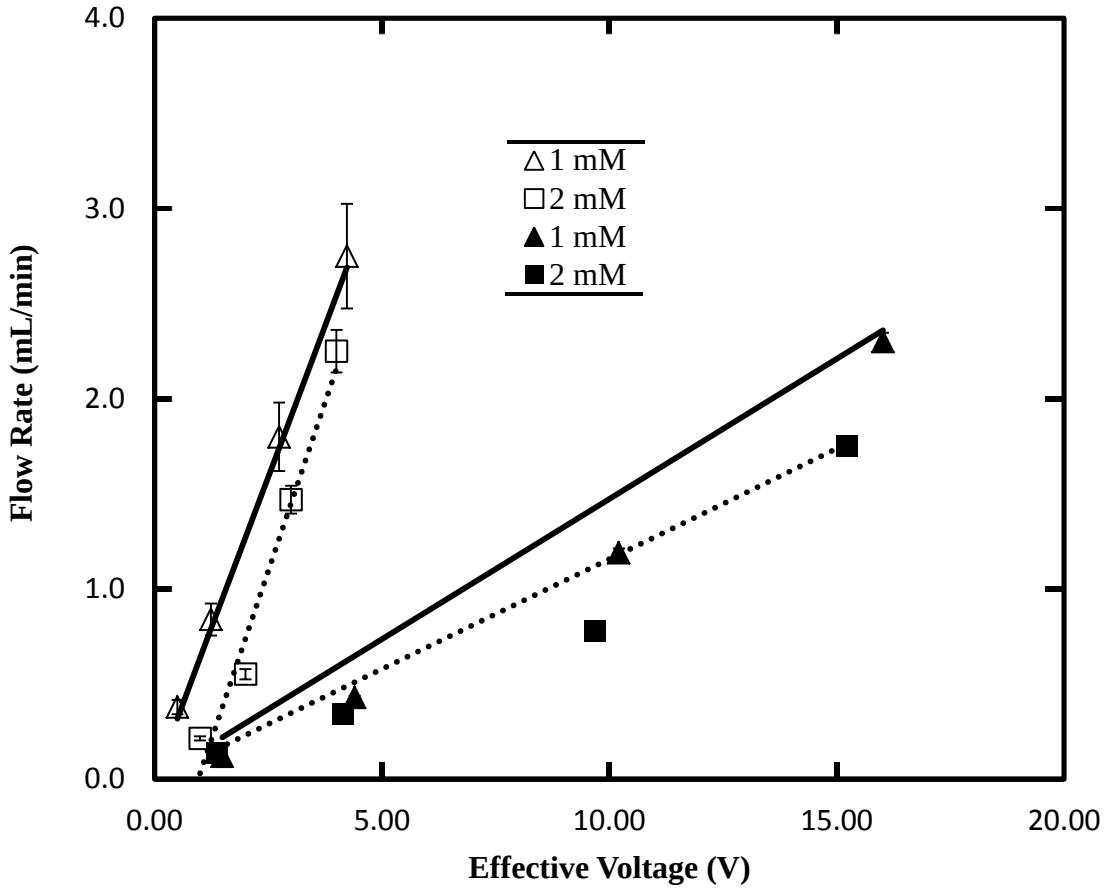

Fig. 10. Measured microcapillary arrays' flow rates plotted against the membrane's effective voltage. Phosphate buffer (closed symbols) and borate buffer (open symbols). Theoretical predictions (solid lines 1mM, dotted lines 2mM). Borate buffer allows for approximately the same flow rate but at a smaller effective voltage due to the increase zeta potential from the higher pH.

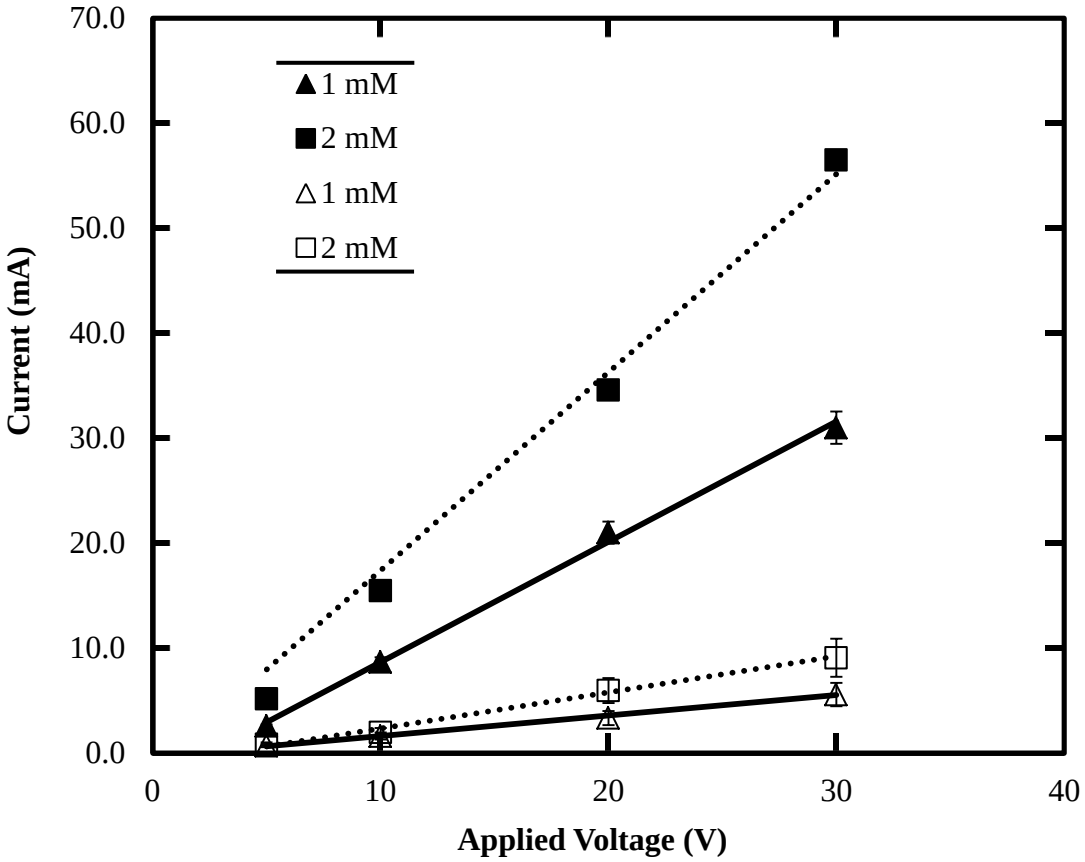

Fig. 11. Measured microcapillary arrays current consumption plotted against applied voltage. Phosphate buffer (closed symbols) and borate buffer (open symbols). Theoretical predictions (solid lines 1mM, dotted lines 2mM). The higher conductivity of the phosphate buffer is the reason for the higher current consumption.

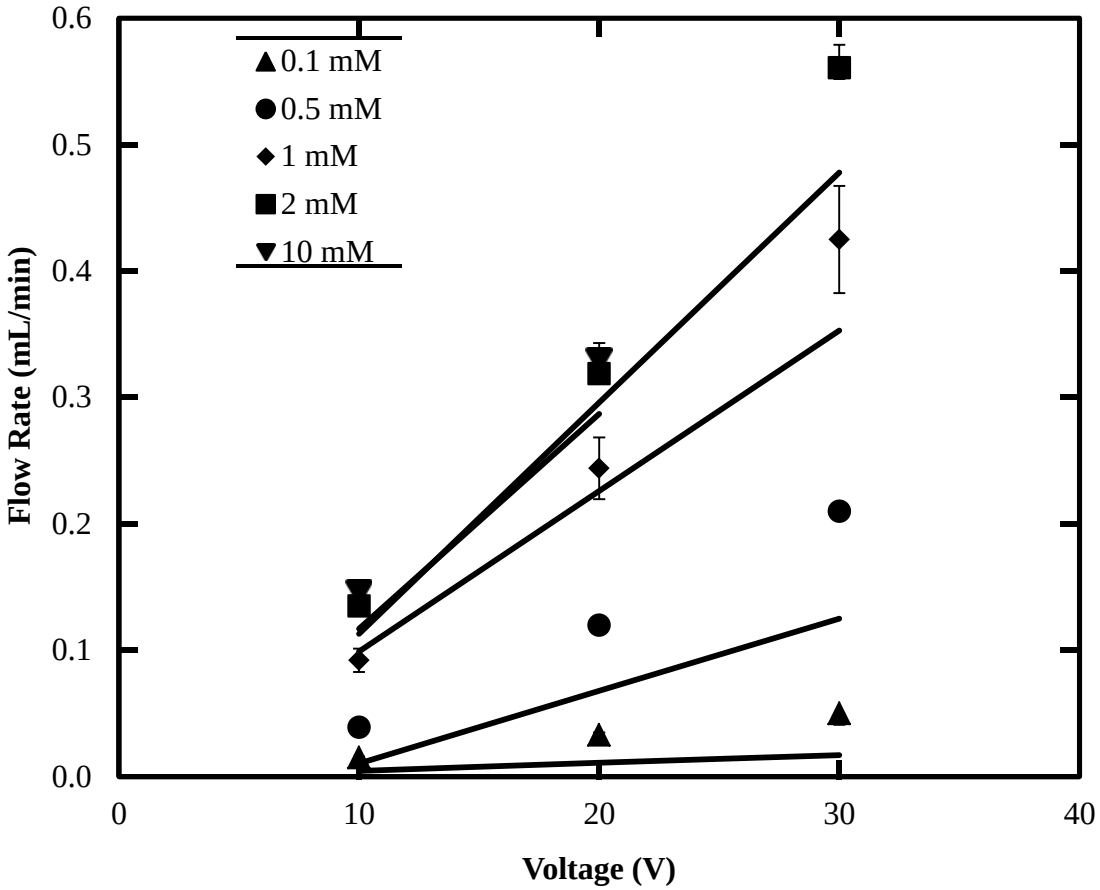

Fig. 12. AAO with SiO_2 coating measured flow rates with theoretical predictions. As shown, flow rate increases with molarity to approximately 2mM. This coincided with experimental results from **[38]**.

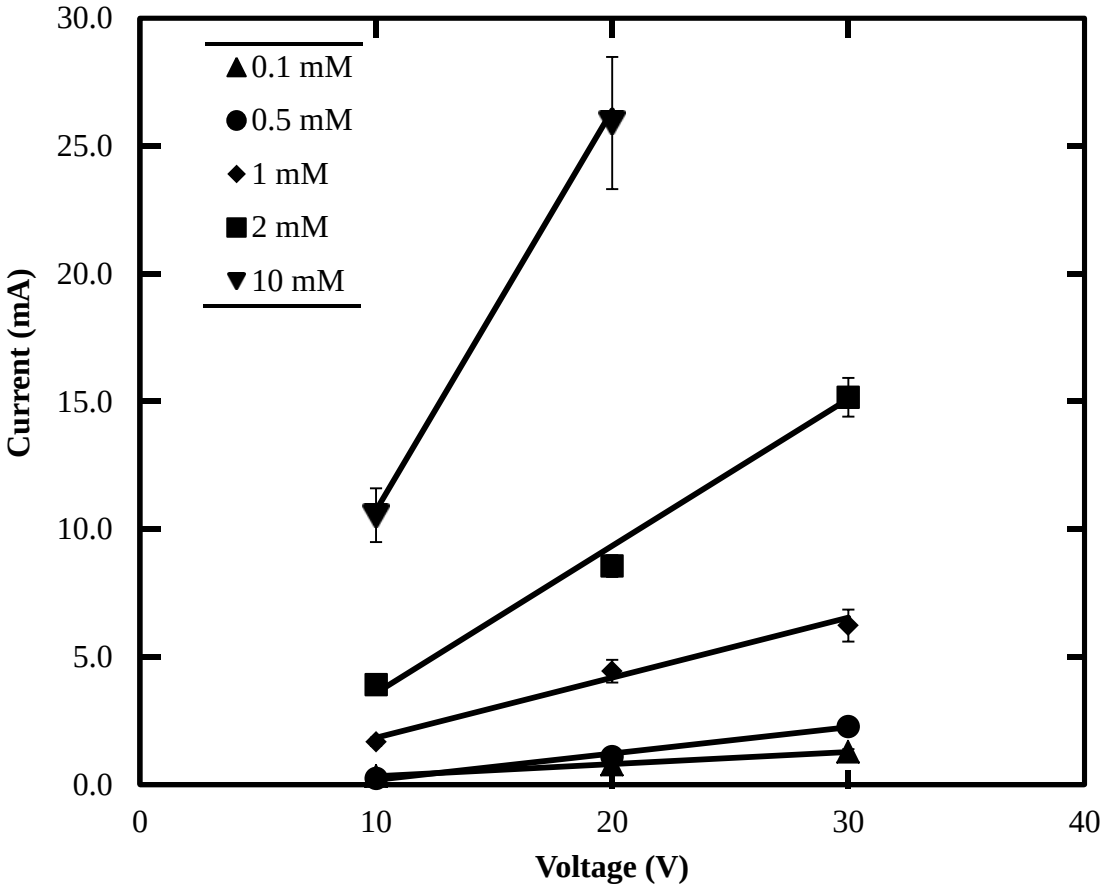

Fig. 13. AAO with SiO_2 coating measured current consumption with theoretical predictions. Increasing the molarity will increase the current consumption and thus a 10mM solution will create a less efficient pump then one at 2mM.

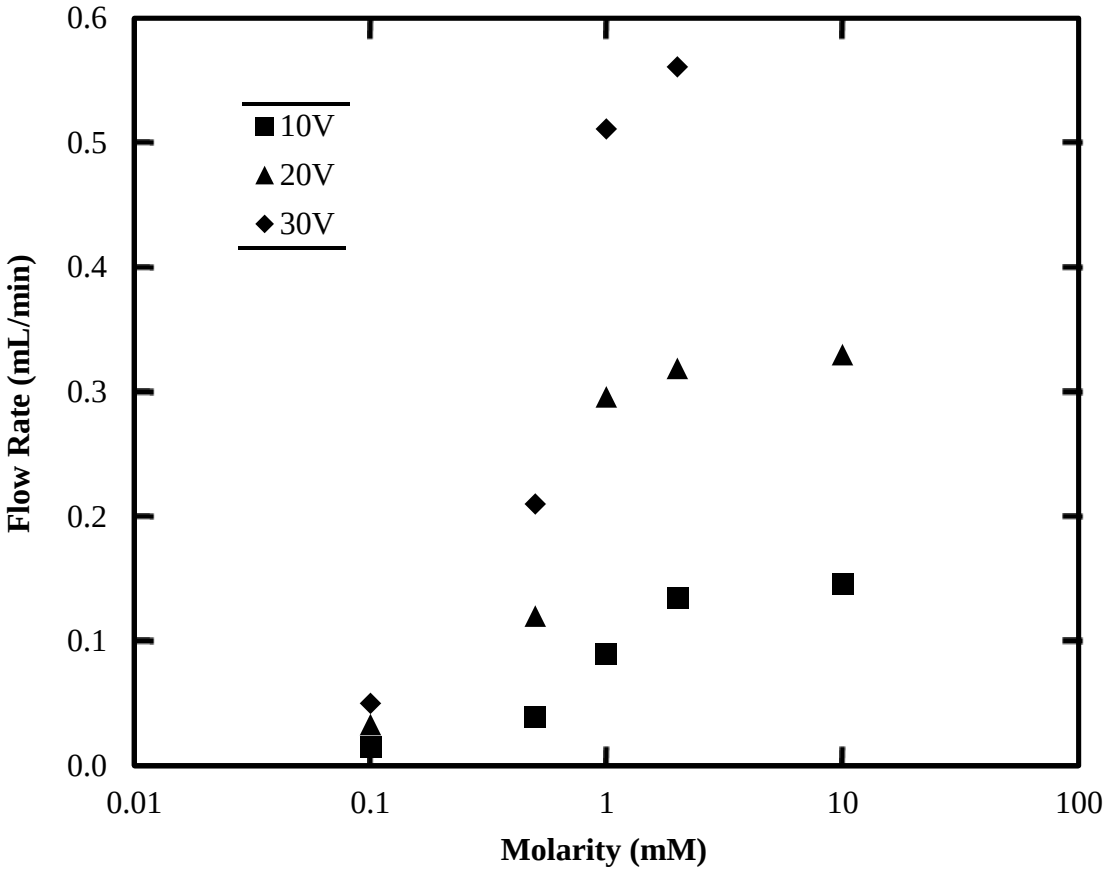

Fig. 14. Flow rates for varying phosphate buffer molarities for SiO_2 coated AAOs. Following the studies by [17], for $10 \geq \kappa a \geq 1$, flow rate decreases as the electric double overlaps. 1mM phosphate buffer ($\kappa a = 8$) has a greater flow rate than a 0.1mM phosphate buffer ($\kappa a = 2$).

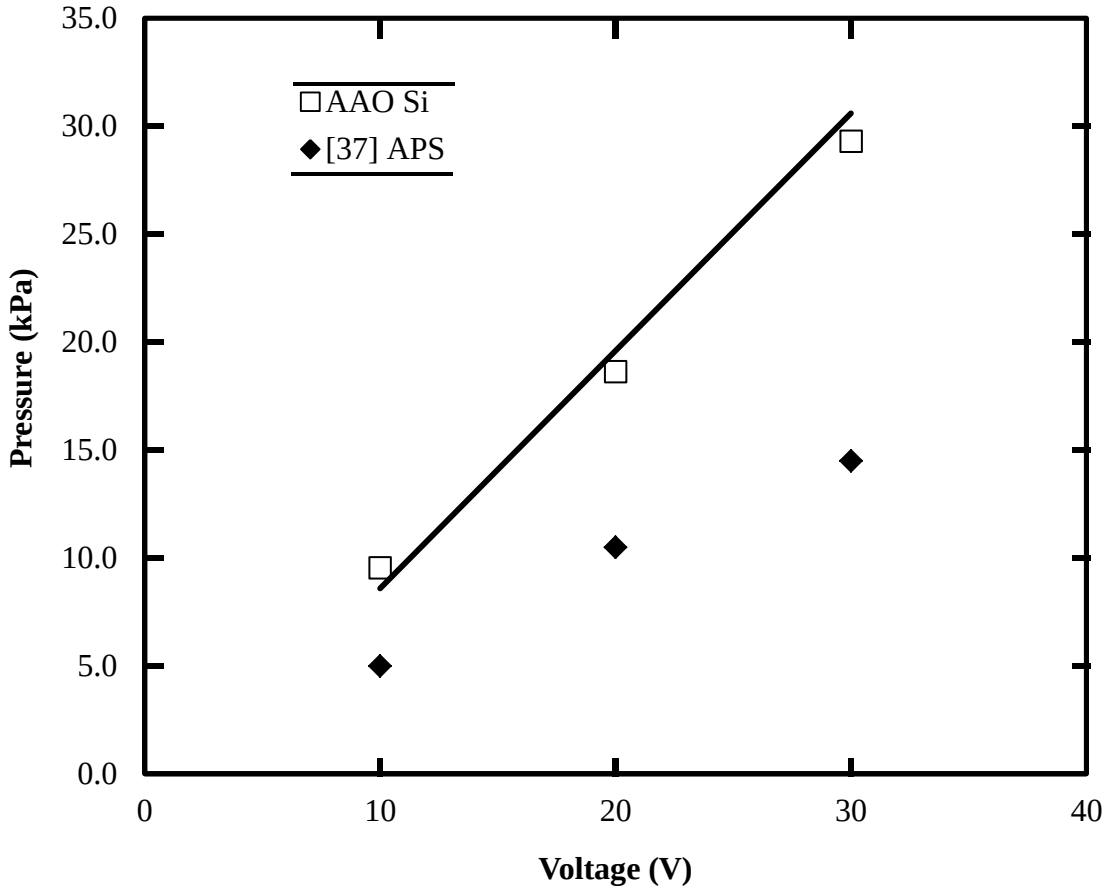

Fig. 15. Pressure measurements for SiO_2 coated AAOs using 1mM phosphate buffer with theoretical predictions (solid line) along with data from [36] using an APS coated AAO with 200nm pores and deionized water. Since maximum pressure is dependent on the inverse of the pore size squared, the higher pressure from the 150nm pores is expected.

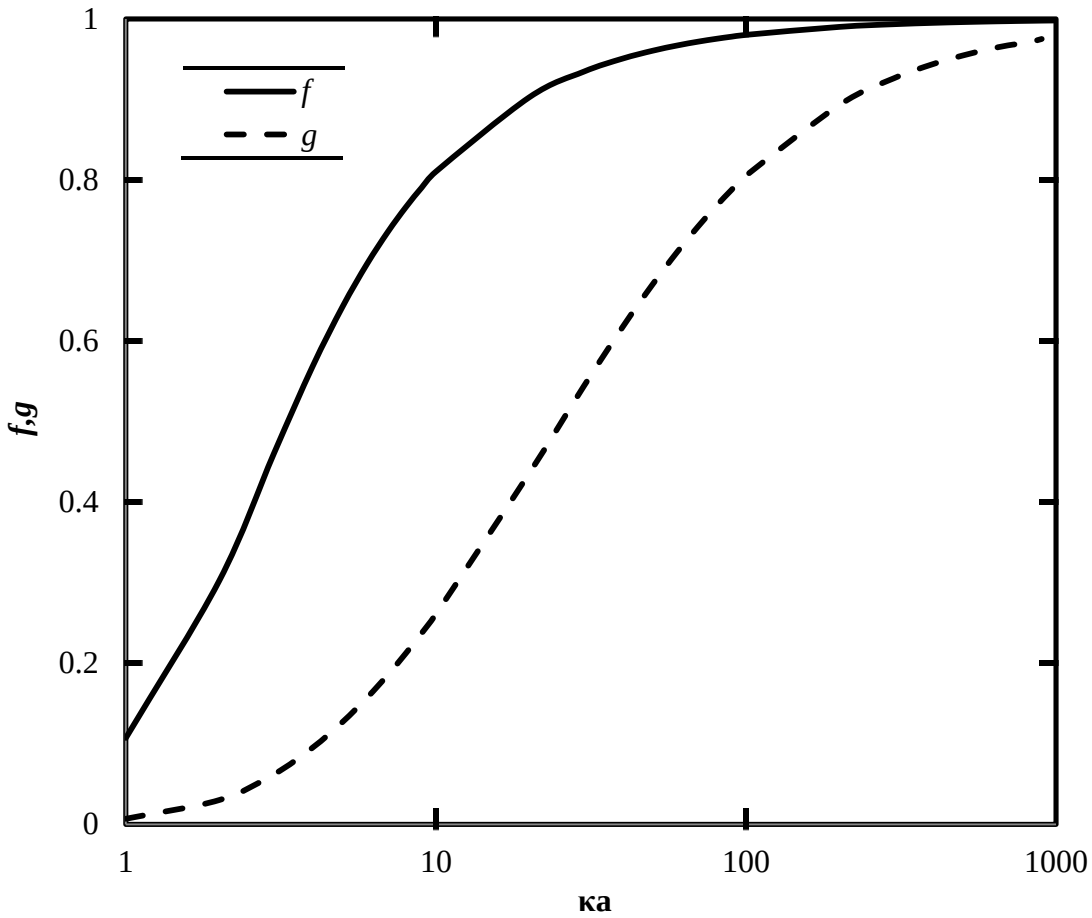

Fig. 16. Dimensionless *f* and *g* values for 1mM phosphate buffer plotted against κa. *f* and *g* become an important factor at low κa values where flow rate and current consumption are dependent on these values. An over prediction of 80% or more can occur if neglecting these terms.

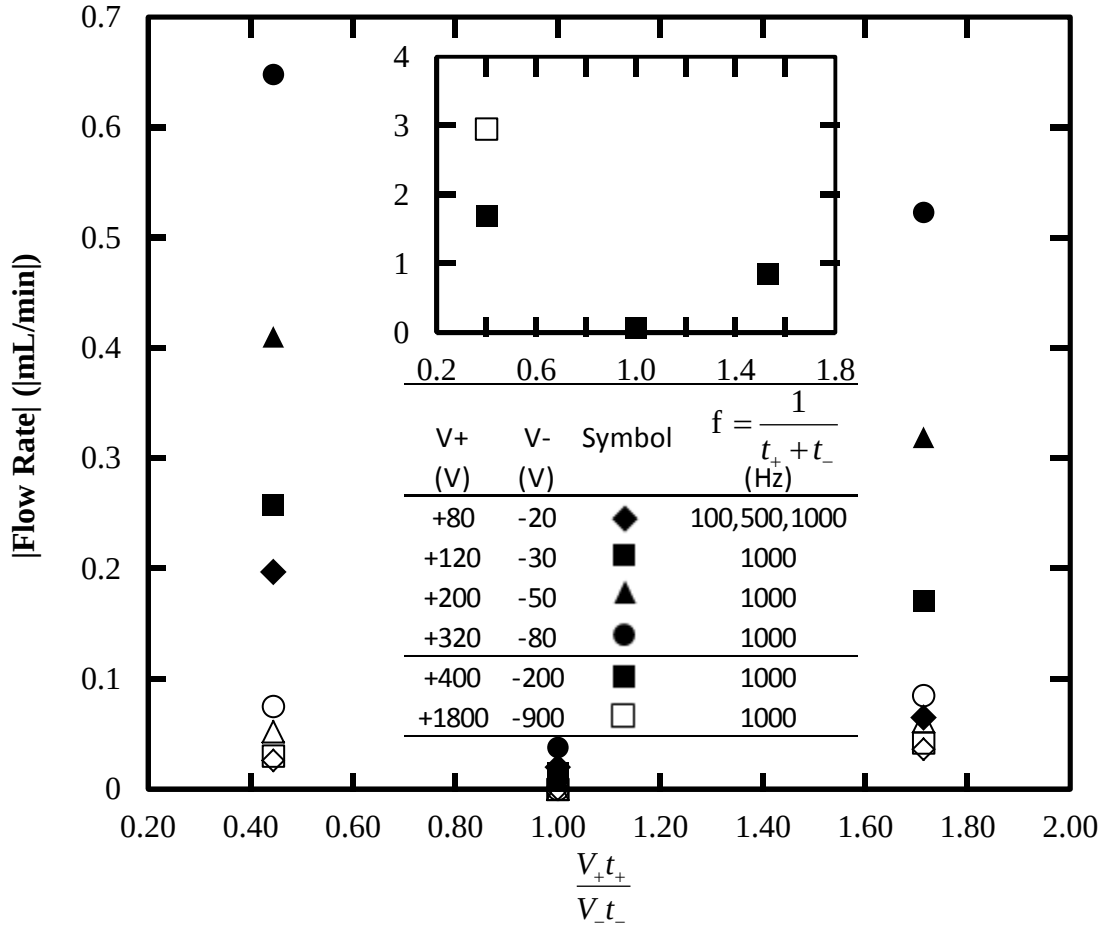

Fig. 17. Measured flow rates due to asymmetric voltage pulsing for SiO_2 coated AAO with 1mM (closed symbols) and 0.1mM (open symbols) phosphate buffer. Inset: High flow rates with maximum amplifier current draw. Asymmetric voltage pulsing is proven to be an effective method for net fluid flow. Asymmetric voltage pulsing also allows a much higher working voltage where constant voltage pumps were stopped at 30V while pulsing allowed up to 1800V for 0.1mM phosphate buffer.

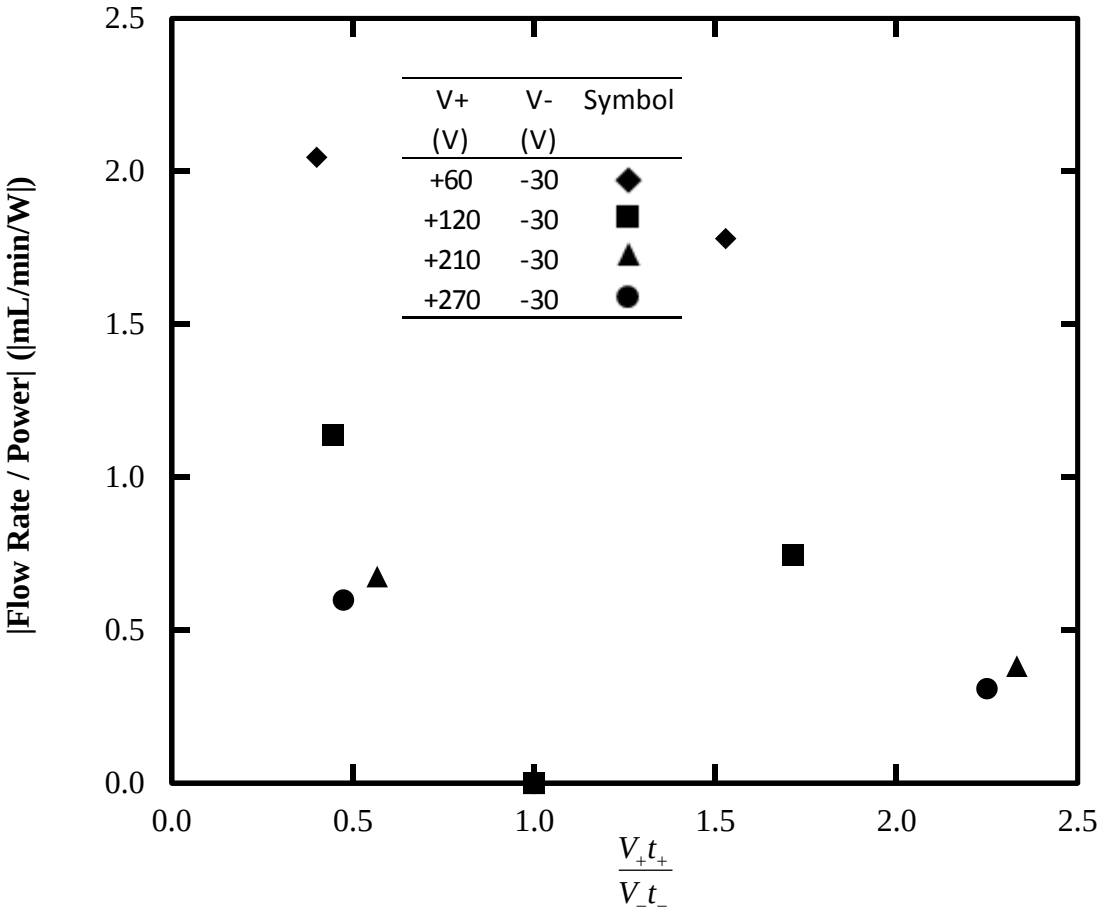

Fig. 18. Pumping characteristics for varying voltage ratios for asymmetric voltage pulsing using an AAO with SiO_2 and 1mM phosphate buffer. A 2:1 voltage ratio allows for the maximum flow rate per supplied power. Though a higher b value allows for a greater flow rate, power consumption increases at a greater rate and thus is not suitable for efficient pumping.

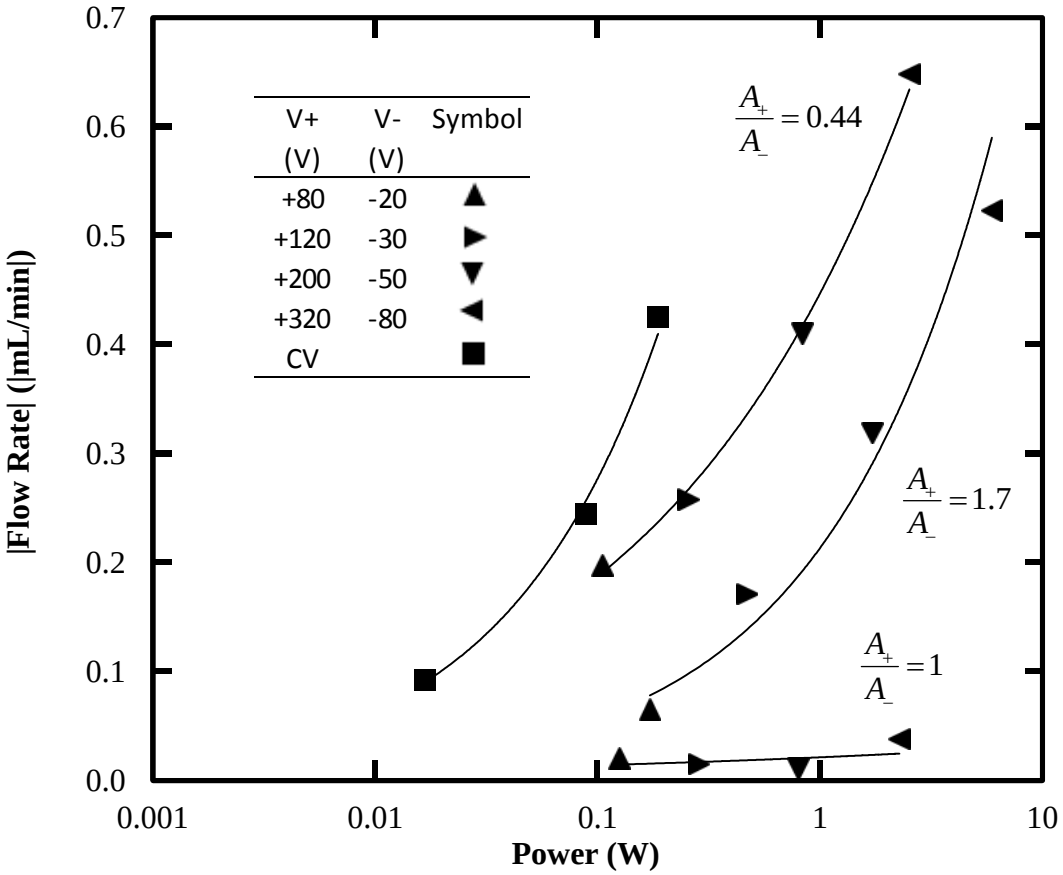

Fig. 19a. Flow rate to power consumption for constant voltage (CV) and asymmetric voltage pulsing for SiO_2 coated AAOs using 1mM phosphate buffer. Plotted with best fit curves, asymmetric voltage pulsing closely resembles the constant voltage curve allowing for predictions of higher flow rate. An area ratio of 0.44 creates the best flow rate per power for asymmetric voltage pulsing due to the lower voltage acting as the driving force.

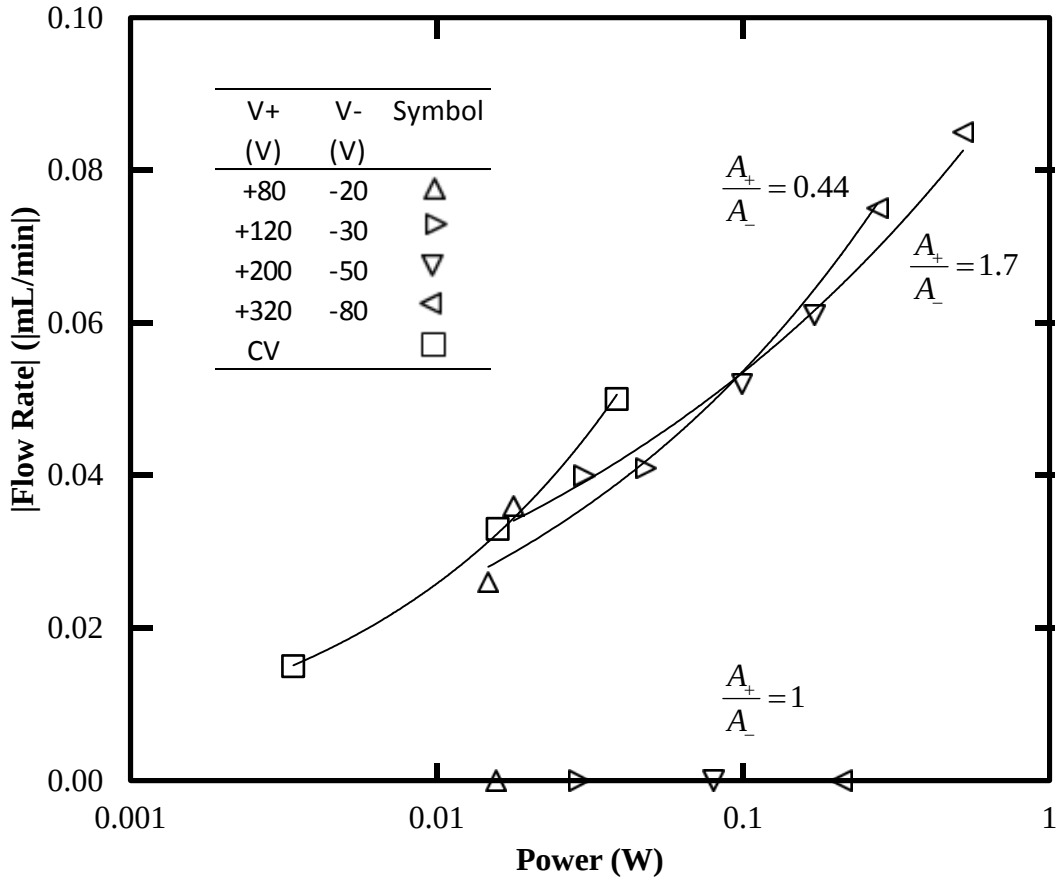

Fig. 20b. Flow rate to power consumption for constant voltage (CV) and asymmetric voltage pulsing for SiO_2 coated AAOs using 0.1mM phosphate buffer. As with the 1mM phosphate buffer, asymmetric voltage pulsing closely resembles constant voltage curves. Again, the area ratio of 0.44 created a slightly better flow rate per unit power though it is not as clear as the 1mM phosphate buffer.

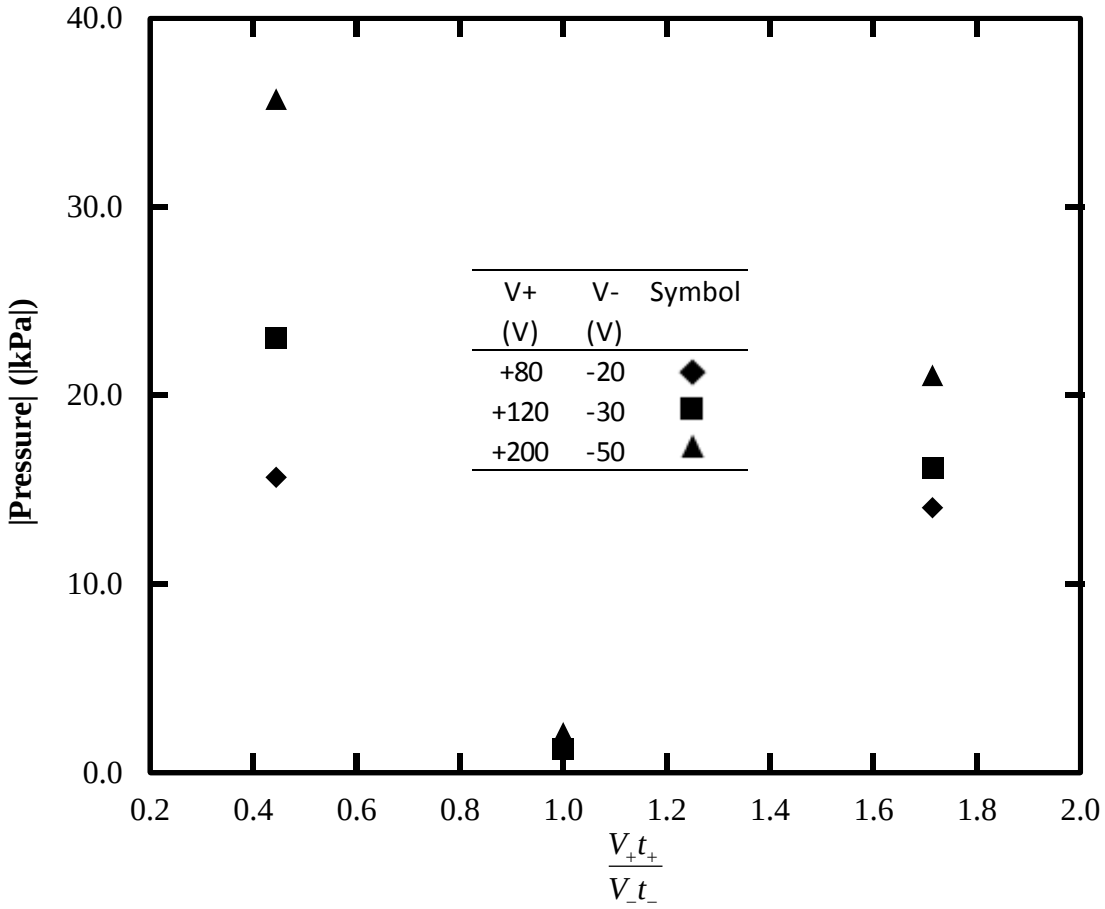

Fig. 21. Measured pressure for asymmetric voltage pulsing for a SiO_2 coated AAO using 1mM phosphate buffer. As expected a higher voltage would increase the maximum pressure. As with flow rate, the negative pulse created a larger driving force and thus a greater maximum pressure.

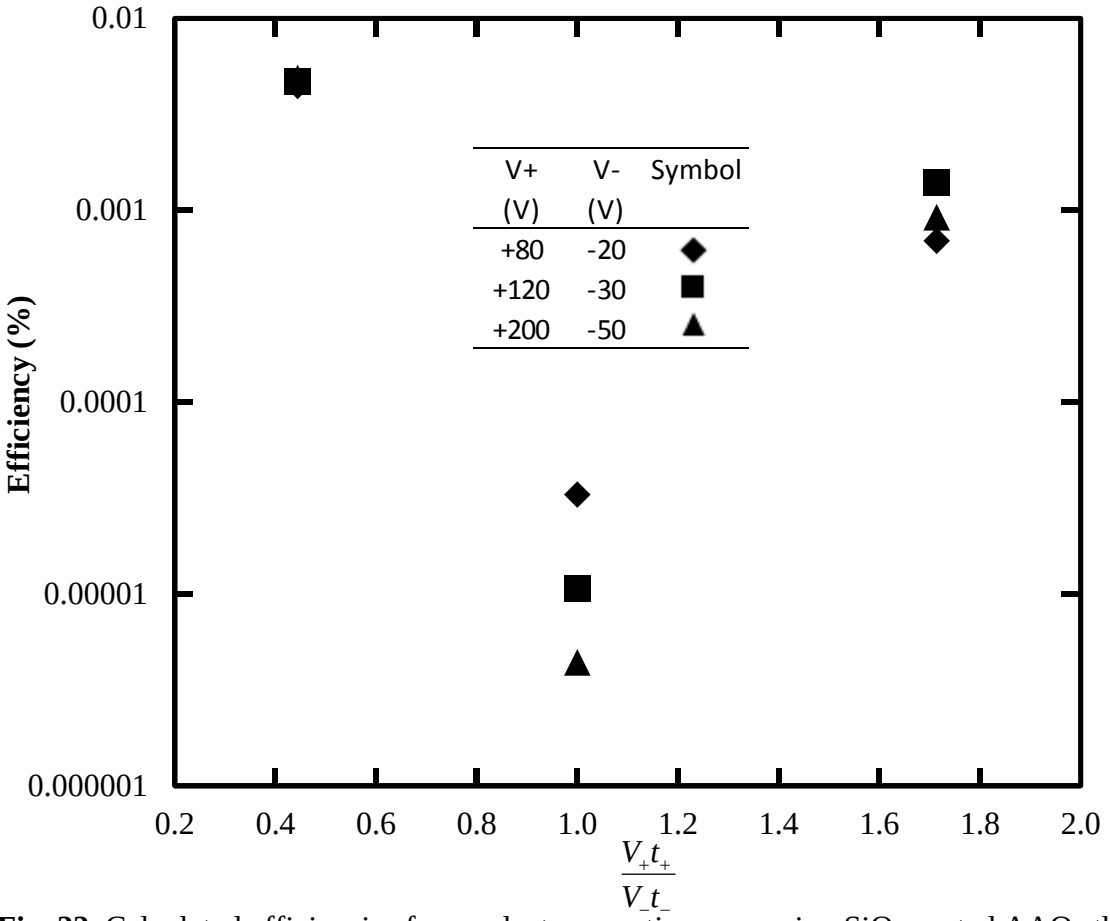

Fig. 22. Calculated efficiencies for an electroosmotic pump using SiO_2 coated AAOs that is driven by asymmetric voltage pulses. Working fluid is 1mM phosphate buffer. The smaller area ratio allows for an efficiency value that is one magnitude away from constant voltage. Interestingly, the non-equal ratios have comparably the same efficiency value but are much more spread out for equal area pulsing.

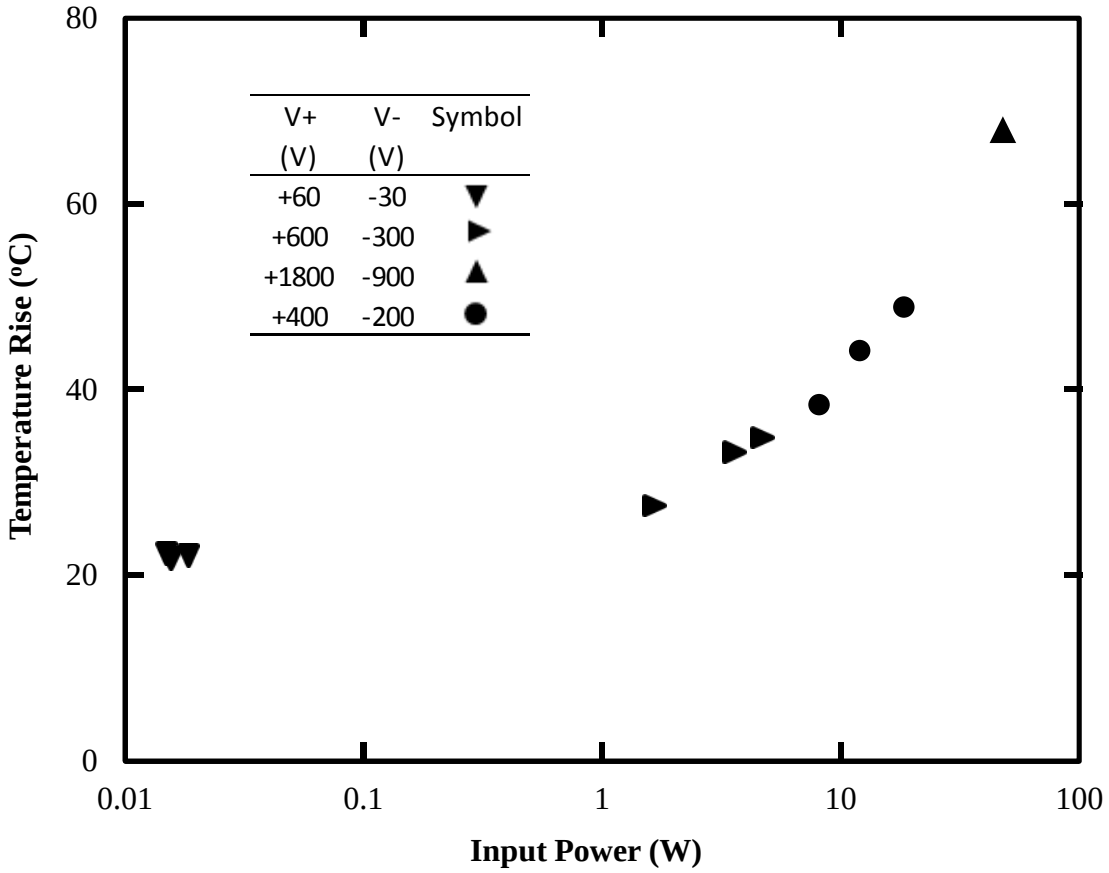

Fig. 23. Fluid temperature rise due to asymmetric voltage pulsing. Triangles are 0.1mM phosphate buffer. Circles are 1mM phosphate buffer. Temperature increase can be attributed to joule heating from the interaction of the electrodes and buffer solution. Large reservoirs and high flow rates may reduce temperature fluctuations.

Chapter 6.

Conclusion

Two types of membranes were analyzed for electroosmotic pumping. Microcapillary arrays were shown to exhibit a normalized flow rate of 0.049 mL/min/V/cm^2. Thickness and pore size reduction would be needed to increase their performance. SiO_2 coated AAOs with and without a Pt coating were also tested with phosphate buffer. The SiO_2 coated AAOs without the Pt coating had a normalized flow rate of 0.102 mL/min/V/cm^2 and with the Pt coating, 1.90mL/min/V/cm^2 which is the highest normalized flow rate to date. It has been shown that by decreasing the distance between the electrode and the membrane can significantly improve the effective voltage and thus increasing the flow rate. Due to higher power consumption, the efficiencies of the SiO_2 coated AAOs dropped compared to other published data.

Asymmetric voltage pulsing has been show to create a net flow in electroosmotic pumps utilizing membranes. The advantage of this method is the stoppage of bubble production at the electrodes. Though this method creates lower flow rates, it may be advantageous towards applications where bubble production would be problematic. By changing the voltage area ratios slightly, a much higher flow rate can occur with limited amounts of bubble generation.

References

[1] R. Probstein, *Physicochemical Hydrodynamics*, 2nd ed. NY: Wiley-Interscience Publication, 1994.

[2] H.-C. Chang and L. Yeo, *Electrokinetically Driven Microfluidics and Nanofluidics*. Cambridge, 2010.

[3] S. Zeng, C. H. Chen, J. C. Mikkelsen, J. G. Santiago, and others, "Fabrication and characterization of electroosmotic micropumps," *Sensors and Actuators B: Chemical*, vol. 79, no. 2–3, pp. 107–114, 2001.

[4] P. Wang, Z. Chen, and H.-C. Chang, "A new electro-osmotic pump based on silica monoliths," *Sensors and Actuators B: Chemical*, vol. 113, pp. 500–509, 2006.

[5] L. Chen, H. Wang, J. Ma, C. Wang, and Y. Guan, "Fabrication and characterization of a multi-stage electroosmotic pump for liquid delivery," *Sensors and Actuators B: Chemical*, vol. 104, no. 1, pp. 117–123, 2005.

[6] S. Yao, D. Hertzog, and J. G. Santiago, "Porous glass electroosmotic pumps: design and experiments," *Journal of Colloid and Interface Science*, vol. 268, pp. 143–153, 2003.

[7] W. Chen, J. H. Yuan, and X. H. Xia, "Characterization and manipulation of the electroosmotic flow in porous anodic alumina membranes," *Analytical chemistry*, vol. 77, no. 24, pp. 8102–8108, 2005.

[8] S. Yao, A. M. Myers, J. D. Posner, K. A. Rose, and J. G. Santiago, "Electroosmotic Pumps Fabricated From Porous Silicon Membranes," *J. Microelectromech. Syst.*, vol. 15, no. 3, pp. 717–728, Jun. 2006.

[9] Z. Cao, L. Yuan, Y.-F. Liu, S. Yao, and L. Yobas, "Microchannel plate electro-osmotic pump," *Microfluidics and Nanofluidics*, Mar. 2012.

[10] Y. Berrouche, Y. Avenas, C. Schaeffer, Hsueh-Chia Chang, and Ping Wang, "Design of a Porous Electroosmotic Pump Used in Power Electronic Cooling," *IEEE Trans. on Ind. Applicat.*, vol. 45, no. 6, pp. 2073–2079, 2009.

[11] C. Bruie, J. D. Posner, T. Fabian, S.-W. Cha, D. Kim, F. Prinz, J. Eaton, and J. G. Santiago, "Water management in proton exchange membrane fuel cells using integrated electroosmotic pumping," *Journal of Power Sources*, vol. 161, pp. 191–202, 2006.

[12] P. Prakash, M. D. Grissom, C. D. Rahn, and A. L. Zydney, "Development of an electroosmotic pump for high performance actuation," *Journal of membrane science*, vol. 286, no. 1–2, pp. 153–160, 2006.

[13] M. J. Pikal, "The role of electroosmotic flow in transdermal iontophoresis," *Advanced drug delivery reviews*, vol. 46, no. 1–3, pp. 281–305, 2001.

[14] L. Chen, J. Ma, and Y. Guan, "Study of an electroosmotic pump for liquid delivery and its application in capillary column liquid chromatography," *Journal of Chromatography A*, vol. 1028, no. 2, pp. 219–226, 2004.

[15] P. C. H. Li and D. J. Harrison, "Transport, manipulation, and reaction of biological cells on-chip using electrokinetic effects," *Analytical Chemistry*, vol. 69, no. 8, pp. 1564–1568, 1997.

[16] S. Levine, J. R. Marriott, G. Neale, and N. Epstein, "Theory of Electrokinetic Flow in Fine Capillaries at High Zeta Potentials," *Journal of Colloid and Interface*

Science, vol. 52, no. 1, pp. 136–149, 1975.

[17] C. L. Rice and R. Whitehead, "Electrokinetic flow in a narrow cylindrical capillary," *The Journal of Physical Chemistry*, vol. 69, no. 11, pp. 4017–4024, 1965.

[18] J. R. Philip and R. A. Wooding, "Solution of the Poisson–Boltzmann Equation about a Cylindrical Particle," *The Journal of Chemical Physics*, vol. 52, no. 2, p. 953, 1970.

[19] S. Yao and J. G. Santiago, "Porous Glass Electroosmotic Pumps: Theory," *Journal of Colloid and Interface Science*, vol. 268, pp. 133–142, 2003.

[20] E. Brunet and A. Ajdari, "Generalized Onsager relations for electrokinetic effects in anisotropic and heterogeneous geometries," *Phys. Rev. E*, vol. 69, no. 1, Jan. 2004.

[21] X. Xuan and D. Li, "Thermodynamic Analysis of Electrokinetic Energy Conversion," *Journal of Power Sources*, vol. 156, pp. 677–684, 2006.

[22] F. H. J. van der Heyden, D. J. Bonthuis, D. Stein, C. Meyer, and C. Dekker, "Electrokinetic Energy Conversion Efficiency in Nanofluidic Channels," *Nano Lett.*, vol. 6, no. 10, pp. 2232–2237, Oct. 2006.

[23] Z. Xu, J. Miao, N. Wang, W. Wen, and P. Sheng, "Digital flow control of electroosmotic pump: Onsager coefficients and interfacial parameters determination," *Solid State Communications*, 2011.

[24] Y.-F. Chen, M.-C. Li, Y.-H. Hu, W.-J. Chang, and C.-C. Wang, "Low-voltage electroosmotic pumping using porous anodic alumina membranes," *Microfluid Nanofluid*, vol. 5, no. 2, pp. 235–244, Dec. 2007.

[25] D. S. Reichmuth, G. S. Chirica, and B. J. Kirby, "Increasing the performance of high-pressure, high-efficiency electrokinetic micropumps using zwitterionic solute additives," *Sensors and Actuators B: Chemical*, vol. 92, no. 1–2, pp. 37–43, 2003.

[26] Y. Ai, S. E. Yalcin, D. Gu, O. Baysal, H. Baumgart, S. Qian, and A. Beskok, "A low-voltage nano-porous electroosmotic pump," *Journal of colloid and interface science*, 2010.

[27] J. M. Burke, C. D. Smith, and C. F. Ivory, "Development of a membrane-less dynamic field gradient focusing device for the separation of low-molecular-weight molecules," *Electrophoresis*, vol. 31, no. 5, pp. 902–909, 2010.

[28] C. W. Lin, S. Yao, J. D. Posner, A. M. Myers, and J. G. Santiago, "Toward orientation-independent design for gas recombination in closed-loop electroosmotic pumps," *Sensors and Actuators B: Chemical*, vol. 128, no. 1, pp. 334–339, 2007.

[29] F. Heuck, P. van der Ploeg, and U. Staufer, "Deposition and structuring of Ag/AgCl electrodes inside a closed polymeric microfluidic system for electroosmotic pumping," *Microelectronic Engineering*, 2011.

[30] A. Brask, D. Snakenborg, J. P. Kutter, and H. Bruus, "AC electroosmotic pump with bubble-free palladium electrodes and rectifying polymer membrane valves," *Lab on a Chip*, vol. 6, p. 280, 2006.

[31] D. Kohlheyer, J. C. T. Eijkel, S. Schlautmann, A. van den Berg, and R. B. M. Schasfoort, "Bubble-Free Operation of a Microfluidic Free-Flow Electrophoresis Chip with Integrated Pt Electrodes," *Analytical Chemistry*, vol. 80, pp. 4111–4118, Jun. 2008.

[32] P. Selvaganapathy, Y. Leung Ki, P. Renaud, and C. H. Mastrangelo, "Bubble-Free Electrokinetic Pumping," *Journal of Microelectromechanical Systems*, vol. 11, no. 5, 2002.

[33] J.-K. Chen, C.-N. Weng, and R.-J. Yang, “Assessment of three AC electroosmotic flow protocols for mixing in microfluidic channel,” *Lab on a Chip*, vol. 9, p. 1267, 2009.

[34] O. M. Stuetzer, “Ion Drag Pressure Generation,” *Journal of Applied Physics*, vol. 30, no. 7, p. 984, 1959.

[35] S. McBride, “Balanced Asymmetric Electronic Pulse Patterns for Operating Electrode-Based Pumps,” U.S. Patent 5,964,99712-Oct-1999.

[36] J. Miao, Z. Xu, and X. Zhang, “Micropumps Based on the Enhanced Electroosmotic Effect of Aluminum Oxide Membranes,” *Advanced Materials*, vol. 19, pp. 4234–4237, 2007.

[37] Y.-F. Chen, Y.-H. Hu, and Y.-I. Chou, “Surface modification of nano-porous anodic alumina membranes and its use in electroosmotic flow,” *Sensors and Actuators B: Chemical*, vol. 145, pp. 575–582, 2010.

[38] S. Vajandar, D. Xu, D. Markov, and J. Wikswo, “SiO2-coated porous anodic alumina membranes for high flow rate electroosmotic pumping,” *Nanotechnology*, vol. 18, 2007.

[39] S. Arulanandam and D. Li, “Determining ζ Potential and Surface Conductance by Monitoring the Current in Electro-osmotic Flow,” *Journal of Colloid and Interface Science*, vol. 225, no. 2, pp. 421–428, May 2000.

[40] P. J. Scales, F. Grieser, T. W. Healy, L. R. White, and D. Y. C. Chan, “Electrokinetics of the silica-solution interface: a flat plate streaming potential study,” *Langmuir*, vol. 8, no. 3, pp. 965–974, 1992.

[41] B. J. Kirby and E. F. Hasselbrink, “Zeta potential of microfluidic substrates: 1. Theory, experimental techniques, and effects on separations,” *ELECTROPHORESIS*, vol. 25, no. 2, pp. 187–202, Jan. 2004.